



5

# Optically-induced reconfigurable photonic lattices for linear and nonlinear control of light

Zhigang<sup>1</sup> Chen and Jianke Yang<sup>2</sup>

<sup>1</sup>TEDA Applied Physics School, Nankai University, Tianjin, China and  
Department of Physics and Astronomy, San Francisco State University  
CA 94132 USA; <sup>2</sup>Department of Mathematics and Statistics  
University of Vermont, VT 05401, USA

## Abstract

*Linear and nonlinear periodic systems are abundant in nature. In optics, a typical example is a closely-spaced waveguide array, in which collective behavior of wave propagation exhibits many intriguing phenomena that have no counterpart in homogeneous media. Even in a linear waveguide array, the diffraction property of a light beam changes due to evanescent*

*coupling between nearby waveguide sites, leading to discrete diffraction. When the waveguide array is embedded in a nonlinear medium, a balance between discrete diffraction and nonlinear self-action gives rise to novel localized states called "discrete solitons". Although waveguide arrays can serve as a test bench for studying many fascinating light behaviors, it has always been a challenge to create or fabricate two-dimensional (2D) waveguide arrays in bulk media, not to mention such arrays with structured defects. Recently, in a series of experimental and theoretical studies, we have "fabricated" closed-spaced waveguide arrays (photonic lattices) by optical induction, as well as lattices with defects akin to optically-induced photonic crystal fibers (PCFs). Such photonic structures have attracted great interest of research due to their novel physics, link to photonic crystals, as well as potential applications in optical switching and navigation. In this Chapter, we provide an overview of experimental demonstration and theoretical understanding of lattice fabrication (including 1D lattices, 2D square lattices and ring lattices, and lattices with structured defects), as well as their linear and nonlinear light guiding properties. In a fabricated uniform lattice, discrete diffraction and self-trapping are demonstrated in a variety of settings, including fundamental discrete solitons, discrete vector solitons, discrete dipole solitons, discrete vortex solitons, and necklace-like solitons. Furthermore, we demonstrate the formation of 1D and 2D lattices with single-site negative defects, and linear bandgap guidance in these structures. In particular, ring-shaped periodic index lattices with a low-index core are optically-induced, resembling antiresonant microstructured fibers or photonic bandgap fibers. Our work brings about the possibility for optical "fabrication" of reconfigurable photonic structures as a new type of optical material for beam shaping and light routing.*

## **1. Introduction**

In the last several years, there has blossomed an interest in the study of collective behavior of wave propagation in closely-spaced nonlinear waveguide arrays [1, 2]. Even in linear propagation, the diffraction property of a light beam in the waveguide array (called discrete diffraction) is distinctively different from that in homogeneous media. When the nonlinear effect of the light beam becomes significant, a balance between discrete diffraction and nonlinear self-focusing gives rise to localized states of light better known as "discrete solitons" [3]. Discrete solitons (DSs) have been predicted to exist in a variety of other nonlinear systems such as biology, solid state physics, and Bose-Einstein condensates, but a convenient way to demonstrate such soliton states is to employ a fabricated or optically-induced waveguide array in nonlinear optics. Indeed, the first experimental demonstration of DSs was carried out in fabricated

---

one-dimensional (1D) AlGaAs semiconductor waveguide arrays [4, 5]. Recently, it has been suggested that DSs could also form in optically-induced waveguide arrays [6]. This soon led to various experimental observations of DSs in such waveguide arrays established with optical induction, either via coherent beam interference [7-9] or via amplitude modulation of a partially coherent beam [10, 11]. Meanwhile, in addition to fundamental discrete solitons, vortex discrete solitons have also been predicted theoretically [12, 13] and demonstrated experimentally [14, 15]. In all these studies, the localization of a light beam in uniform periodic structures results from the combined effect of lattice discreteness and nonlinear self-trapping, and the formation of a DS could be considered as a self-induced *nonlinear* photonic defect mode.

On the other hand, it is well known that one of the unique and most interesting features of the photonic band-gap (PBG) structures is a fundamentally different way of waveguiding by defects in otherwise uniformly periodic structures as opposed to conventional guidance by total internal reflection or soliton-induced nonlinear self-guiding. Such a waveguiding property has been demonstrated with an “air-hole” in photonic crystal fibers (PCF) for optical waves [16, 17], in an isolated defect in two-dimensional arrays of dielectric cylinders for microwaves [18], and recently in all-solid PCF with a lower-index core [19, 20]. In fact, PBG guidance has been studied for a wide range of spectra, and laser emission based on photonic defect modes (DMs) has been realized in a number of experiments [21, 22]. In photonic crystals and PCF, bandgap guidance is associated with the time-domain frequency modes where the propagation constant is imaginary (i.e., propagation forbidden – band gaps). Within the gaps, light can be localized by defects that support evanescent defect states [16-22]. Similarly, the analyses of how a monochromatic light field distributes in waveguide lattices often focus on the bandgaps of spatial frequency modes (i.e., propagation constant vs. transverse wave vector) [23-25]. In one-dimensional (1D) fabricated semiconductor waveguide arrays, previous experiments have investigated nonlinearly induced escape from a defect state [26] and interactions of discrete solitons with structural defects [27]. In optically-induced photonic lattices such as those induced in photorefractive crystals, theoretical work has also predicted the existence of linear DMs [28, 29]. However, direct observation of PBG guidance at different bandgaps of optically induced lattices with structured defects has remained a challenge until our recent experimental demonstrations [30-32]. In these studies, the localization of a light beam results from linear bandgap guidance or the formation of a *linear* photonic defect mode.

In this Chapter, we present a brief overview of our recent work on the optical fabrication of 1D and 2D periodic lattices and lattices with single-site negative defects, as well as their linear and nonlinear light guiding properties. In

uniform photonic lattices, various nonlinear discrete solitons will be presented; in a defective photonic lattice, linear guided modes (defect modes) will be reported. We emphasize the difference between the two cases: for discrete solitons in periodic lattices, the probe beam experiences high nonlinearity but the lattice beam does not; whereas for light confinement by defects embedded in otherwise uniform lattices, both the probe beam and the lattice beam experience no or only weak nonlinearity. We discuss how to “fabricate” these lattices by the method of optical induction, with lattice structures varying from 1D to 2D, from square to ring, and from uniform to defective lattices. In the uniform lattices, we demonstrate the formation of fundamental nonlinear discrete solitons, trains of such solitons in stripe or necklace shape, as well as vector, dipole and vortex solitons in lattices. Different from other experiments in which the lattice is created by *coherent* multi-beam interference [7-9], in our setting the lattices are created by spatial amplitude modulation of a partially spatially *incoherent* optical beam. This in turn enables stable lattice formation due to suppression of incoherent modulation instability [33, 34], and also brings about the possibility to create other lattice structures such as ring lattices and lattices with single-site defects which cannot be done by the interference method. In fact, it is in our partially coherent stable lattices that detailed features of transition from discrete diffraction to formation of discrete solitons were clearly demonstrated [10, 11]. In the defective lattices, we demonstrate the formation of linear defect modes and bandgap guidance. We predict theoretically and demonstrate experimentally PBG guidance in optically-induced photonic lattices with a single-site negative defect. In such a defective lattice, the refractive index at the defect is lower than that in the surrounding “rods” (akin to an “air defect” in photonic crystals or hollow-core PCF, and much alike all-solid low-index-core PCF). Spatial confinement of the probe beam at different wavelengths during its linear propagation through the defect is clearly observed, although the defect is repulsive and the beam itself has no nonlinear self-action. Such guidance of light in the negative defect arises from linear propagation of the defect modes formed in the spatial bandgap of the photonic lattice, which is fundamentally different from linear guidance by total internal reflection or nonlinear self-guidance as in a spatial soliton. In addition, we show that the “guided” patterns by the defect display fine spatial structures such as dipole and vortex cells which arise from the DM excited at higher bandgaps. Our optical induction of reconfigurable photonic lattices with defects not only has direct linkage to technologically important systems of periodic structures such as PCF, but also brings about the possibility for studying, in an optical setting, many novel phenomena in periodic systems beyond optics such as defect healing, eigenmode splitting, and nonlinear mode coupling which have been intriguing scientists for decades.

## 2. “Fabrication” of 1D uniform lattices and nonlinear discrete trapping

With today’s nano-fabrication technology, to create a closed-spaced 1D waveguide array on a substrate material is not a problem. As an example, such waveguide structures have been fabricated with AlGaAs semiconductor materials or LiNbO<sub>3</sub> crystals. In fact, the first experimental demonstration of DSs was carried out in fabricated 1D semiconductor waveguide arrays [4, 5]. Yet, it has always been a challenge to create or fabricate 2D or 3D waveguide arrays in bulk media. Motivated by observation of DSs in higher dimensions, it has been suggested that waveguide lattices could be optically-induced in a photorefractive crystal [6]. Indeed, experimental observations of DSs in such waveguide lattices were established with optical induction by sending multiple interfering beams into the nonlinear crystal [7-9]. A typical example of such an experimental setting is illustrated in Fig. 2.1, along with the observation of discrete trapping in 1D waveguide lattices.

The coherent multiple-beam interference method has many disadvantages for creating photonic lattice structures. For instance, the induced lattice tends to be more sensitive to ambient perturbation. Furthermore, when the lattice

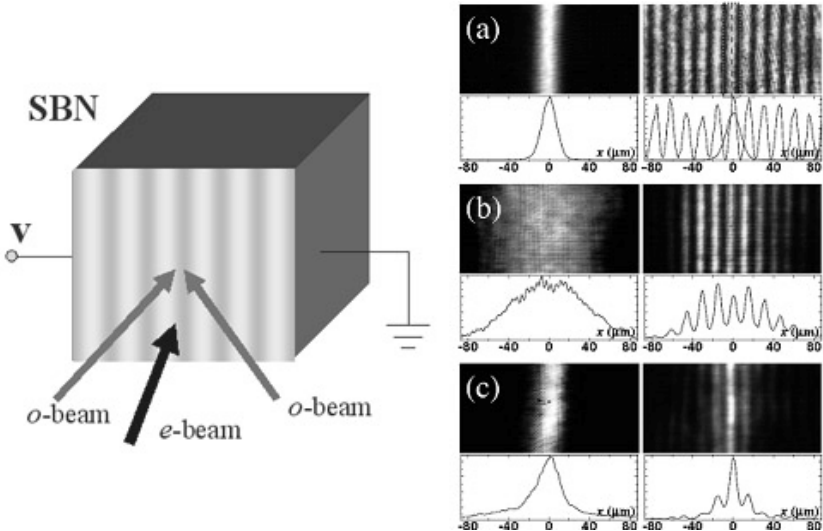


**Figure 2.1.** Left panel: Illustration for optical induction of 1D waveguide lattices in a biased photorefractive crystal by the interference method. SBN: strantium barium niobate. Right panels: Typical experimental results of discrete trapping of an optical beam in optically induced 1D lattices (after Ref. [9]).

beam itself experiences an appreciable nonlinearity, it becomes considerably more susceptible to modulation instability and the lattice structure cannot be stable either when the lattice spacing is too small or the nonlinearity is too high. More importantly, the interference method cannot generate more complicated lattice structures such as binary lattices or lattices with structured defects. In view of that, we proposed a different method of optical induction which is based on the periodic amplitude modulation of a partially coherent optical beam. This incoherent amplitude-modulation method made possible the first experimental demonstration of 2D solitonic lattices in a 3D bulk crystal [35]. In what follows, we describe our experimental arrangement for the lattice induction, and our theoretical understanding of such induction method in the 1D case, while the approach can be easily modified to explain the generation of 2D square lattices.

The experimental setup for our study is illustrated in Fig. 2.2. Our experiments are performed in a biased photorefractive crystals (typically SBN:60, with  $r_{33}\sim 280$  pm/V and  $r_{13}\sim 24$  pm/V) illuminated by a laser beam (either Coherent argon ion laser  $\lambda=488$  nm or solid-state laser  $\lambda=532$  nm) passing through a rotating diffuser and an amplitude mask. The biased crystal provides a self-focusing or -defocusing noninstantaneous nonlinearity [36]. The rotating diffuser turns the laser beam into a partially spatially incoherent beam with controllable degree of spatial coherence, as first introduced in experiments of incoherent optical solitons [37, 38]. The amplitude mask provides spatial modulation after the diffuser on the otherwise uniform beam, which exhibits a periodic intensity pattern at the input face of the crystal [35]. This partially coherent and spatially modulated beam is used as our *lattice beam*. Another beam split from the same laser or a different laser but without going through the diffuser and the mask is used as our *probe beam*, propagating along with the lattice. As explained below, both the lattice beam and the probe beam can be made to undergo linear or nonlinear propagation through the biased crystal by adjusting their intensity, polarization, or wavelengths. The two beams at input and output facets of the crystal are monitored separately with a CCD camera. In addition, a white-light background beam illuminating from the top of the crystal is typically used for fine-tuning the photorefractive nonlinearity [35-38].

We emphasize that, the method of optical induction of waveguide lattices and nonlinear self-trapping of discrete solitons in photorefractive crystals is directly related to the anisotropic property of the photorefractive nonlinearity. In general, in an anisotropic photorefractive crystal, the nonlinear index change experienced by an optical beam depends on its polarization as well as on its intensity. Under appreciable bias conditions, i.e., when the photorefractive screening nonlinearity is dominant, this index change is approximately given by

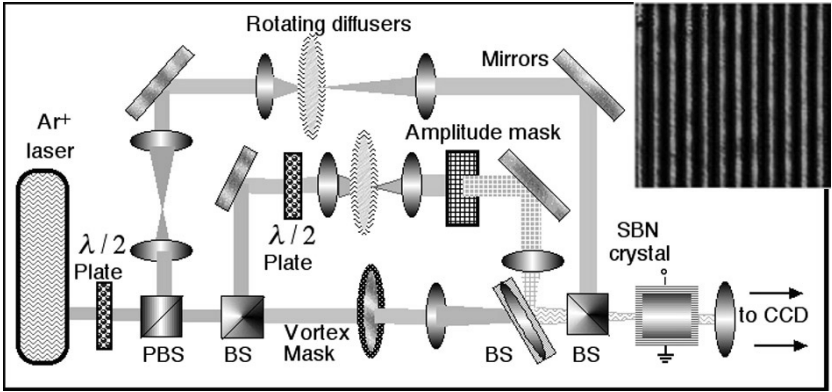


**Figure 2.2.** Experimental setup for optical induction of waveguide lattices in a biased photorefractive crystal by amplitude modulation of a partially coherent beam. PBS: polarizing beam splitter; SBN: strontium barium niobate. Top path is for incoherent background illumination, middle path is for the modulated beam to induce the lattice, and bottom path is for the probe which can be a Gaussian or vortex (when the vortex mask is present) beam. The right insert shows a typical picture of 1D photonic lattice created by optical induction.

$\Delta n_e = [n_e^3 r_{33} E_0 / 2](1 + I)^{-1}$  and  $\Delta n_o = [n_o^3 r_{13} E_0 / 2](1 + I)^{-1}$  for extraordinarily-polarized (*e*-polarized) and ordinarily-polarized (*o*-polarized) beams respectively [6-11]. Here  $E_0$  is the applied electric field along the crystalline *c*-axis (*x*-direction), and  $I$  is the intensity of the beam normalized to the background illumination. Due to the difference between the nonlinear electro-optic coefficient  $r_{33}$  and  $r_{13}$ ,  $\Delta n_e$  is more than 10 times larger than  $\Delta n_o$  under the same experimental conditions in a SBN:60 crystal. Thus, if the lattice beam is *o*-polarized while the probe beam is *e*-polarized, the lattice beam would experience only weak nonlinear index change, and the lattice in this case could be considered as undergoing *linear* propagation. In Fig. 2.2, the insert shows a typical example of a 1D lattice pattern created in our experiment. The lattice has a spatial period of about 40  $\mu\text{m}$ , but this spacing can be varied easily from 10 to 100  $\mu\text{m}$  by using different masks or different magnification of imaging. Even for the bias field as high as 3 kV/cm, the lattice structure still remains nearly invariant when exiting the crystal. On the other hand, the polarization of the lattice beam can also be changed to include an *e*-polarized component or to be completely *e*-polarized, which will result in a “mixed” or “flexible” soliton-like nonlinear lattice [10, 35, 39-42]. In our work with discrete solitons and linear defect modes, the lattice beam has its polarization close to be *o*-polarized, thus the lattice beam induces a weak index change for the waveguide arrays. The probe

beam on the other hand is always a coherent  $e$ -polarized beam, but its intensity and/or wavelength can be adjusted so it can undergo linear propagation (for study of linear guidance or linear defect modes) or nonlinear propagation (for study of nonlinear trapping or nonlinear defect modes) as detailed in later sections.

To understand how a periodic lattice can stay stationary during its linear propagation through the crystal, we need to understand how to eliminate the *Talbot effect* (this effect was recently investigated also in discrete systems [43, 44]). The Talbot effect is a phenomenon of coherent light propagation in a homogeneous media with spatially-periodic initial conditions. The phenomenon is that light does not propagate stationarily --- it shrinks and expands as it moves along, and its intensity pattern repeats itself periodically along the propagation direction. Our lattice beam travels in a homogeneous crystal (as it does not feel the probe beam), and its initial condition on the input face of the crystal is periodic (due to the amplitude mask). Because of the Talbot effect, it can not form a stationary lattice. To overcome this difficulty, our idea is to use frequency filtering to remove half of the spatial frequencies in the initial conditions. The filtered lattice beam, when slightly tilted, can propagate stationarily along the crystal; thus, the Talbot effect is eliminated. The stationary lattice so obtained is the basis for our further experiments on probe beams.

To analytically understand the elimination of the Talbot effect by frequency filtering, we consider the following non-dimensionalized Schroedinger equation for linear coherent-light propagation in a 1D homogeneous media under paraxial approximation:

$$iU_z + U_{xx} = 0. \quad (2.1)$$

Here  $U$  is the envelope function of the light beam,  $z$  is the propagation direction, and  $x$  is the transverse direction. To reproduce the Talbot effect, we take the initial condition as a periodic function

$$U_0(x) = A_0 + A_2 \cos 2x, \quad (2.2)$$

where  $A_0$  and  $A_2$  are constants. If we take  $A_0 = A_2 = 1$ , then the intensity pattern of this initial condition is shown in Fig. 2.3 (1<sup>st</sup> row, left column), and its frequency spectrum shown in Fig. 2.3 (2<sup>nd</sup> row, left column). The solution of Eq. (2.1) with this initial condition is

$$U(x, z) = A_0 + A_2 \cos 2x e^{-4iz}. \quad (2.3)$$

Clearly, the intensity of this solution changes periodically along the propagation direction  $z$  (with period  $\pi/2$ ), see Fig. 2.3 (third row, left column).



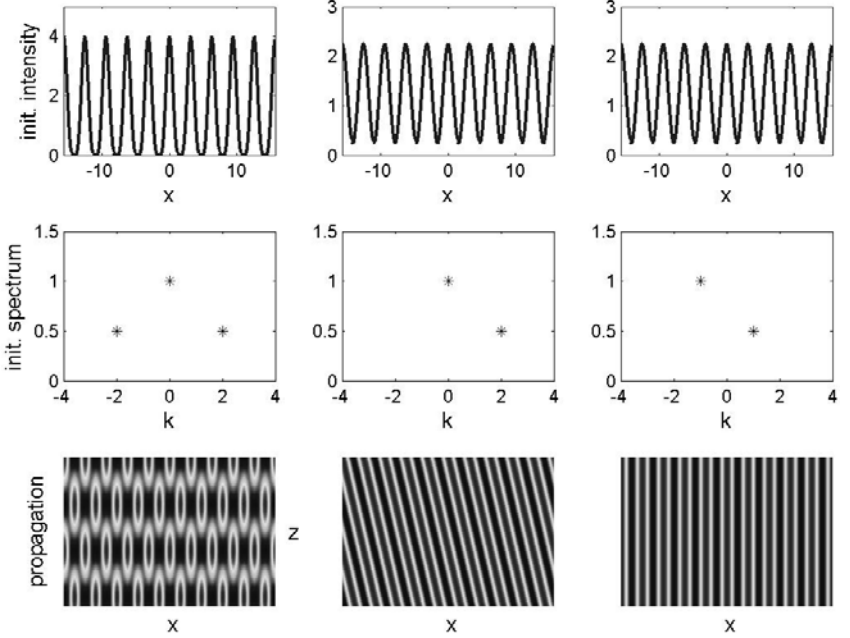


**Figure 2.3.** Elimination of the Talbot effect by frequency filtering and beam tilting. First row: initial intensity patterns; second row: spectrum of the initial fields; third row: evolution plots with the initial conditions as shown in the top row. Left column: for periodic initial conditions (2.2) with no frequency filtering; middle column: for initial conditions (2.2) with frequency filtering; right column: for initial conditions (2.2) with both frequency filtering and beam tilting.

This is the familiar Talbot effect. To eliminate this effect, we first filter out the left half of the initial spectrum, i.e., we remove the  $k = -2$  frequency in Fig. 2.3 (2<sup>nd</sup> row, left column). The initial condition after this filtering is

$$U_0(x) = A_0 + \frac{1}{2}A_2e^{2ix}, \quad (2.4)$$

and its intensity as well as spectrum are shown in Fig. 2.3 (1<sup>st</sup> and 2<sup>nd</sup> rows, middle column). The solution for this initial condition becomes

$$U(x, z) = A_0 + \frac{1}{2}A_2e^{2ix-4iz}. \quad (2.5)$$

A remarkable fact about this solution is that it does not exhibit the Talbot effect any more! Rather, the lattice propagates uniformly --- but at a small angle

(see Fig. 2.3, third row, middle column). To further remove this slanted propagation, we only need to tilt the initial lattice beam a little bit. This beam tilting amounts to multiplying the initial condition (2.4) by a phase gradient, i.e.

$$U_0(x) = (A_0 + \frac{1}{2} A_2 e^{2ix}) e^{-ix}, \quad (2.6)$$

whose intensity profile remains the same as that of (2.4), but its spectrum is shifted (see Fig. 2.3, 1<sup>st</sup> and 2<sup>nd</sup> rows, right column). The solution for this initial condition is

$$U(x, z) = (A_0 e^{-ix} + \frac{1}{2} A_2 e^{ix}) e^{-iz}, \quad (2.7)$$

whose propagation now is stationary (see Fig. 2.3, third row, right column) ! Thus, by combining frequency filtering and beam tilting, we completely removed the Talbot effect and obtained a lattice beam whose intensity pattern is perfectly uniform upon propagation. It is noted that using similar ideas, two-dimensional stationary lattices can be generated as well.

Experimentally, what we did to obtain a stationary 1D lattice was just that. First a beam was launched through an amplitude mask to create a transverse-periodic intensity pattern (Fig. 2.2). When this pattern was imaged onto the input face of the crystal, an aperture was used at the Fourier plane to do spatial filtering. After that, the lattice beam was tilted slightly so that the lattice pattern propagates collinearly with one of the crystalline axes. With such combined use of spatial frequency filtering and beam tilting, the lattice pattern remains stationary during linear propagation through the crystal, or even so when weak nonlinearity is applied provided that the lattice beam is *o*-polarized. When an *e*-polarized probe beam is sent into such a lattice, 1D discrete diffraction and discrete trapping similar to those shown in Fig. 2.1 were realized. However, our results on 2D discrete trapping using the amplitude modulation method [10] are significantly better than those previously obtained with the multiple beam interference method [8]. Furthermore, our method makes it possible to induce nonlinear photonic lattices and lattices with structured defects.

### 3. “Fabrication” of 1D defective lattices and linear bandgap guidance

If a periodic lattice has a local defect, this defect can affect the propagation of a probe beam in a fundamental way. For instance, if the defect is repulsive (negative), i.e. the lattice intensity at the defect is lower than that in neighboring lattice sites, the defect can guide a linear localized mode (defect mode), which is counter-intuitive. The physical mechanism for this unusual

light guiding is the repeated Bragg reflections, rather than the conventional total internal reflections. This is analogous to light transmission in air-hole photonic crystal fibers (PCFs). The PCFs need to be drawn mechanically, which is an expensive process. It would be very appealing, from the point of view of both fundamental research and physical applications, to *optically* create periodic lattices with local defects. The question is: can this be possible?

To explore this question, we prepare an initial periodic lattice with a single-site negative defect using amplitude masks. To keep this defective lattice propagating stationarily along the crystal, we apply the frequency filtering and beam tilting techniques as before. However, we find that if this propagation is linear, those techniques are not enough to maintain the defect and keep the lattice stationary in our experimental conditions. The defect tends to be washed out at the exit face of the crystal. In order to maintain the defect, we need to employ additional techniques. One technique is to introduce a small amount of nonlinearity into the lattice beam (by setting its polarization so that it contains a small amount of *e*-polarized component), so the lattice is slightly “mixed” rather than “fixed” [42]. This weak nonlinearity helps to prevent the nearby lattice sites from spreading into the defect site. Another technique is to introduce partial incoherence into the lattice beam (by letting the lattice beam go through a rotating diffuser). This partial incoherence reduces the nonlinear interference between lattice sites, which stabilizes the lattice. When all these techniques are utilized, we finally succeeded in maintaining a defect in the otherwise uniform lattice which remains nearly stationary. The experimental result is shown in Fig. 3.1(a, b). Here Fig. 3.1 (a) is the input of the 1D lattice with a defect (lattice spacing about 42  $\mu\text{m}$ ). The polarization angle is about 8% relative to the *o*-axis, and the propagation distance is 20 mm. At the bias field of 1.1kV/cm, the output is shown in Fig. 3.1(b). It is seen that the defect is well maintained throughout propagation. After such a lattice is “fabricated”, its light guiding property can be studied. To do so, we launch a low-intensity *e*-polarized probe beam into the defect. The experimental result is shown in Fig. 3.1 (c, d). It can be seen that after 20mm propagation, most of the probe-beam energy is still confined inside the negative defect. This is remarkable, as without the defect, the probe beam would strongly scatter to nearby lattice sites due to discrete diffraction. The negative defect traps the probe beam against discrete diffraction, which is quite unusual.

To further understand the linear light-guiding property of a negative defect, we study this light guiding theoretically next [28, 29]. The non-dimensionalized model for a probe beam propagating in this defective lattice is

$$iU_z + U_{xx} - \frac{E_0}{1 + I_L(x)} U = 0, \quad (3.1)$$

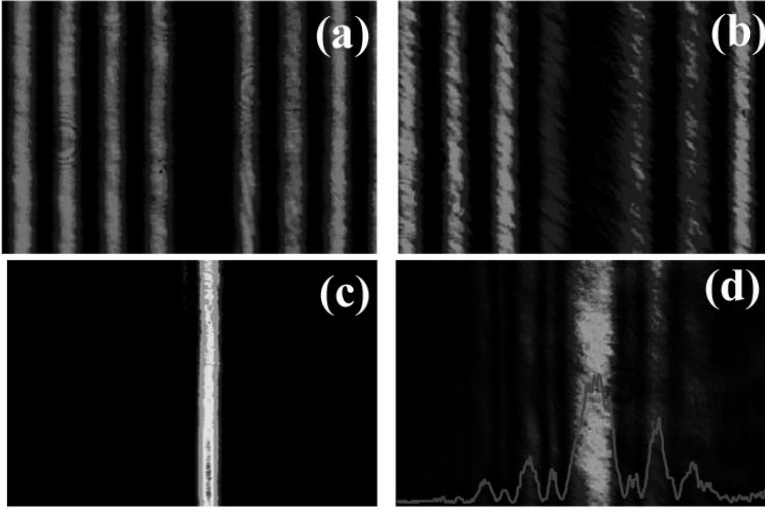


**Figure 3.1.** Transverse intensity patterns of the lattice beam at crystal input (a) and output (b) with a single-site defect, and those of probe beam at input (c) and output (d) after 20-mm of propagation through the defect channel. Lattice spacing: 42  $\mu\text{m}$ . Bias field: 1.1 kV/cm. (after Ref. [32]).

Where  $E_0$  is the applied bias field,  $I_L(x) = I_0 \cos^2 x(1-f_D(x))$  is the lattice intensity containing a defect,  $I_0$  is the lattice peak intensity, and  $f_D(x) = \exp(-x^8/128)$  accounts for the single-site negative defect. If we take  $I_0 = 3$ , this defective lattice is shown in Fig. 3.2(a). A surprising fact is that this negative defect supports localized defect modes of the form  $U(x,z) = u(x)\exp(-i\mu z)$ , where  $\mu$  is the propagation constant (defect-mode eigenvalue). These eigenvalues versus  $E_0$  are shown in Fig. 3.2(b). It is seen that these eigenvalues all lie in the gaps between Bloch bands. None of them exists in the semi-infinite bandgap (total internal reflection region). As  $E_0$  increases, these modes disappear from lower bandgaps, and appear in higher bandgaps. These modes can be symmetric or anti-symmetric. Representative profiles on three different defect-mode branches of Fig. 3.2(b) are shown in Fig. 3.2 (c, d, e). These modes can be quite localized (see (e)), or quite broad (see (d)), depending on where in the bandgap they lay, and which branch they belong to. In particular, the experimentally observed defect mode in Fig. 3.1 (d) strongly resembles that shown in Fig. 3.2(c), which lies in the first bandgap (between the two lowest

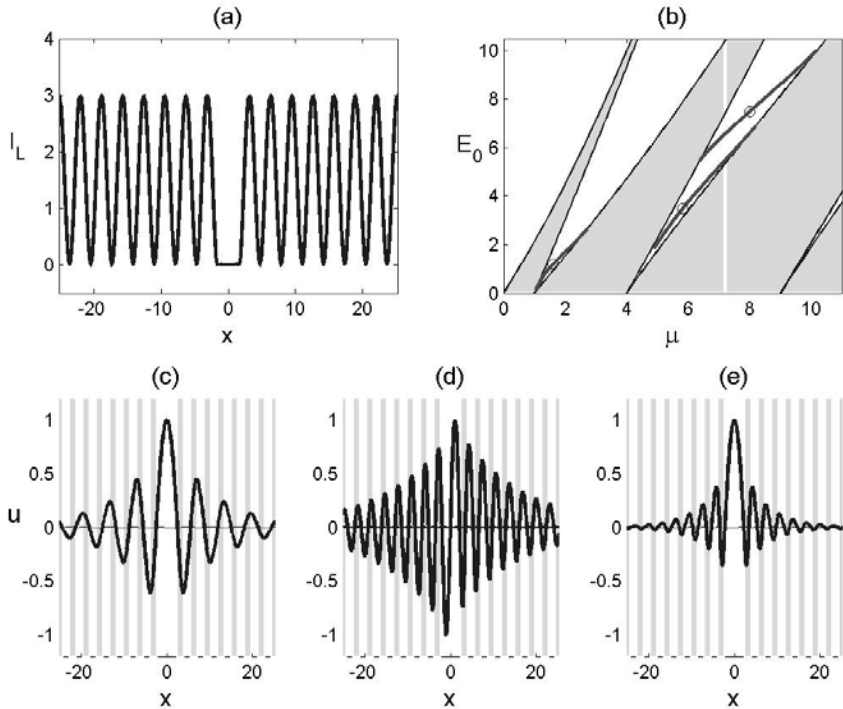


**Figure 3.2.** (a) Lattice intensity profile with  $I_0 = 3$ ; (b) applied bias field parameter  $E_0$  versus the propagation constant  $\mu$ ; the shaded regions are Bloch bands. (c)–(e) three defect modes at  $(E_0, \mu)$  points  $(1.2, 1.604)$ ,  $(3.5, 5.812)$  and  $(7.5, 7.997)$ , marked by circles in (b). The shaded stripes indicate the locations of the lattice’s peak intensities (after Ref. [28]).

Bloch bands). A signature of this defect mode is that neighboring intensity peaks are separated by one lattice spacing. In higher bandgaps, neighboring peaks of defect modes are separated by half a lattice spacing instead [see Fig. 3.2 (d, e)]. In all these defect modes, neighboring intensity peaks are out of phase though.

The theoretical results shown in Fig. 3.2 predict that as the applied bias field increases, defect modes shift from lower bandgaps to higher bandgaps. We have confirmed this prediction experimentally. The experimental results are shown in Fig. 3.3. Here the output probe beams at four different bias fields are shown, with the input being a symmetric Gaussian beam. The top panel is the intensity plot, while the bottom panel shows the interferogram of the probe beam with a plane wave. We see that at a low bias field (0.5 kV/cm), the output

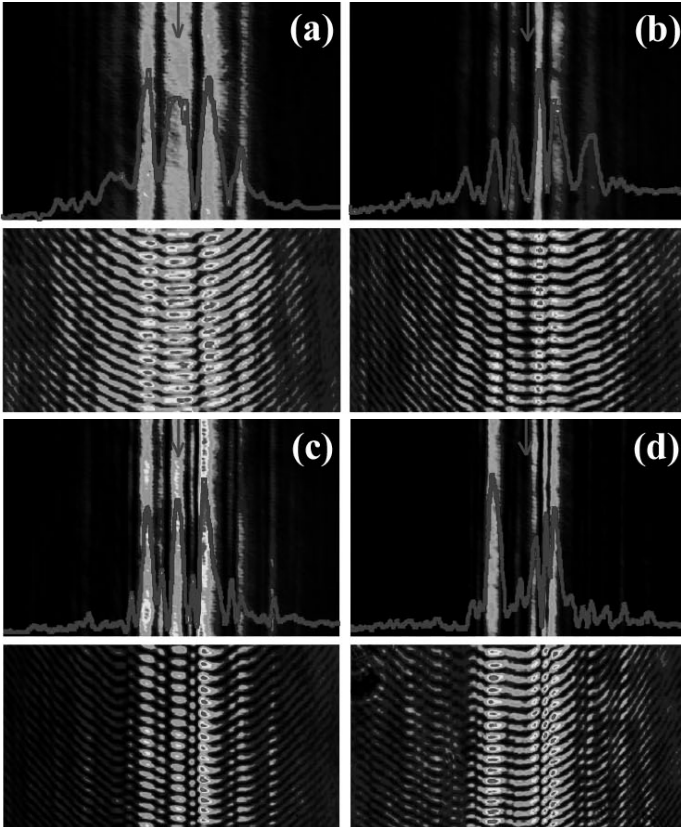


**Figure 3.3.** Top: output probe beam. Bottom: interferogram of the probe beam with a plane wave. From left to right: bias field is 0.5, 1.1, 1.7, and 2.3 kV/cm for the normalized lattice intensity of 0.25 (after Ref. [32]).

probe beam [Fig. 3.3(a)] exhibits several properties of a defect mode located in the first bandgap, including that the probe beam maintains a central lobe at the defect site, and there is only one intensity peak with respect to each lattice site away from the defect, and there is an anti-phase relation between the central lobe in the defect and two side lobes in the tail since the interference fringes interleave at off-site locations. At a higher bias field of 1.1 kV/cm, the probe beam scatters away from the defect site, indicating that the Gaussian beam cannot evolve into a defect mode under this condition [Fig. 3.3 (b)]. However, as the bias field is increased to 1.7 kV/cm, the beam evolves into a defect mode in the second bandgap [Fig. 3.3 (c)]. This can be examined not only from

the intensity pattern which shows double peaks corresponding to each lattice site except for the central defect site [see also Fig. 3.2(e)], but also from the interferogram which shows the anti-phase relation for adjacent peaks. At an even higher bias (2.3 kV/cm), the probe beam scatters away from the defect site again [Fig. 3.3 (d)]. These results clearly illustrate a defect-mode transition from the first bandgap [Fig. 3.3 (a)] to the second bandgap [Fig. 3.3 (c)] as we increase the bias field. The theory also predicts anti-symmetric defect modes between bias fields of Figs. 3.3 (a) and (c), see Fig. 3.2 (d). However, such anti-symmetric modes can not be excited by symmetric Gaussian input beams.

#### 4. “Fabrication” of 2D uniform square lattices and nonlinear discrete trapping

The experimental setup for “fabrication” of 2D lattices is the same as that illustrated in Fig. 2.2. A partially spatially incoherent light beam is generated by converting an argon ion laser beam into a quasi-monochromatic light source with a rotating diffuser. A biased photorefractive crystal is employed to provide a saturable self-focusing noninstantaneous nonlinearity. To generate a 2D-waveguide lattice, we use an amplitude mask to spatially modulate (in two orthogonal transverse directions) the otherwise uniform incoherent beam after the diffuser. The mask is then imaged onto the input face of the crystal, thus creating a pixel-like input intensity pattern which remains stationary through the crystal after proper spatial filtering and beam tilting as explained in section 2. This lattice beam can be turned into either extraordinarily or ordinarily polarized with a half-wave plate as necessary. A Gaussian beam split from the same laser but without passing through the diffuser is used as the probe beam propagating along with the lattice. For the vortex experiment, the probe beam is sent through a transmission vortex mask (bottom path), and then focused onto the crystal input face, propagating collinearly with the lattice.

Typical examples of 2D square lattices created by optical induction in our crystal with both *o*-polarized and *e*-polarized beams are shown in Fig. 4.1. Our experiment shows that the linear square lattices generated with *o*-polarized partially coherent beams are stable and robust, even at small lattice spacing of 20  $\mu\text{m}$  or less [Fig. 4.1(a)]. However, to create a nonlinear (solitonic) square lattice with the *e*-polarized beam, it is a challenge to obtain a stable lattice without distortion at such small lattice spacing. In addition, due to the anisotropic self-focusing nonlinearity, the pixels (or waveguides) tend to merge in the *y*-direction if the square lattice is oriented in horizontal/vertical directions. The diagonal orientation of the square lattice (i.e., its principal axes oriented in the  $45^\circ$  directions relative to *x*- and *y*-axis) favors stable lattice formation due to enlarged *y*-separation between pixels, especially when the lattice spacing is small.

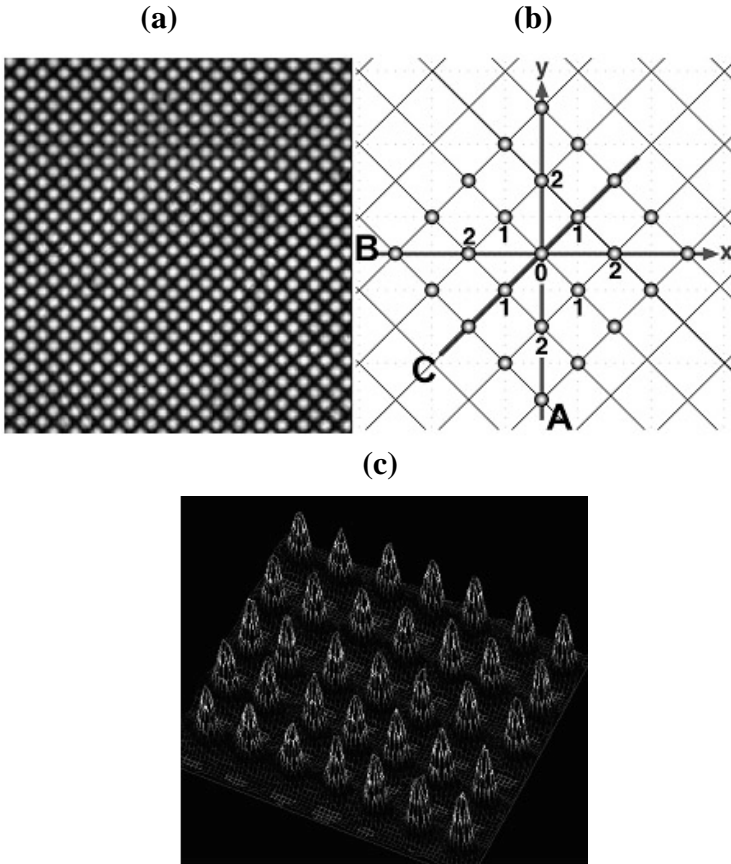


**Figure 4.1.** Optically induced 2D square lattices by amplitude modulation of a partially coherent beam in a biased photorefractive crystal. (a) is the 2D linear lattice with lattice spacing of  $20\ \mu\text{m}$ . (b) illustrates the probe beam location relative to the lattice as used in the following experiments. (c) shows a typical 3D plots of the 2D nonlinear lattice (with lattice spacing  $70\ \mu\text{m}$ ) formed as arrays of pixel-like spatial solitons (after Ref. [35]).

Figure 4.1(a) shows a stable 2D *linear* lattice with  $20\ \mu\text{m}$  spacing created with an *o*-polarized beam. If the polarization is changed to be *e*-polarized, the lattice is strongly distorted at this spacing in the nonlinear regime. The reason for this is quite intuitive. The *e*-polarized lattice experiences a strong nonlinear self-focusing effect, and thus each lattice site tends to form a pixel-like soliton itself. When the lattice spacing is small, the size of each soliton pixel is also



small. With the photorefractive screening nonlinearity, the formation of solitons must satisfy certain conditions better described by the soliton-existence curve [45, 46]. In essence, forming a smaller soliton requires a higher nonlinearity, which is usually achieved by increasing the bias field across the nonlinear crystal. However, with a higher nonlinearity, an  $e$ -polarized lattice beam tends to suffer from stronger modulation instability as driven by noise such as defects and striations in the crystal, which afflicts the formation of a stable solitonic lattice. This is why we introduce partial coherence in the lattice beam. As has been previously predicted [33] and experimentally demonstrated [34, 47-49], partial coherence can result in suppression of modulation instabilities. Therefore, to create a nonlinear lattice with enhanced stability, it often requires fine-tuning of the experimental parameters such as the bias field, lattice spacing, as well as lattice beam intensity and spatial coherence. At larger lattice spacing, nonlinear lattices of pixel-like spatial solitons were realized in our earlier experiments. Figure 4.1(c) shows a typical example of a stable nonlinear lattice (at  $70\ \mu\text{m}$  spacing) obtained by the method of incoherent amplitude modulation [35]. In fact, such nonlinear solitonic lattices with spacing as small as  $37\ \mu\text{m}$  were realized in our later experiments by fine-tuning the nonlinearity [50].

In what follows, we shall use the *linear* or “fixed” square lattice oriented diagonally for the experiments on nonlinear discrete trapping and linear photonic defect modes. Illustration of lattice orientation and excitation location of the probe beam is shown in Fig. 4.1(b). For fundamental 2D discrete solitons, this probe beam is focused with a circular lens into a 2D Gaussian beam and launched into one of the lattice sites, while for demonstrating 1D discrete soliton trains, the beam is focused with a cylindrical lens into a quasi 1D stripe beam. In experiments with dipole and vector lattice solitons, the probe beam is split into two by a Mach-Zehnder interferometer. The two beams exiting from the interferometer are combined with the lattice beam, propagating collinearly through the crystal. When the two beams from the interferometer are made mutually incoherent by ramping a piezo-transducer mirror at a fast frequency, the vector components are realized by overlapping the two beams onto the same lattice site, where each beam itself is coherent and experiences a strong self-focusing nonlinearity [51]. When the two beams from the interferometer are made mutually coherent with a controlled phase relation, dipole-like discrete solitons are investigated by launching the two in-phase or out-of-phase beams into two neighboring lattice sites such as those marked as “0” and “2” in Fig. 4.1(b) [52]. If the two probe beams are launched into two inter-site locations (i.e., two off-site locations between “0 and “2”), they can also form symmetric or anti-symmetric (twisted) soliton states depending on their relative phase [53].

## 5. Discrete fundamental solitons

First, we present our results on 2D fundamental discrete solitons. A stable waveguide lattice (spacing  $20\ \mu\text{m}$  and the FWHM of each lattice site about  $10\ \mu\text{m}$ ) is induced by an o-polarized partially coherent beam. Then, a probe beam (whose intensity is 4 times weaker than that of the lattice) is launched into one of the waveguide channels, propagating collinearly with the lattice. Due to weak coupling between closely spaced waveguides, the probe beam undergoes discrete diffraction when the nonlinearity is low, whereas it forms a 2D discrete soliton at an appropriate level of high nonlinearity. Typical experimental results are presented in Fig. 4.2, where the first two photographs show the Gaussian-like probe beam at the crystal input [Fig. 4.2(a)] and its linear diffraction at the crystal output after 8 mm of propagation [Fig. 4.2(b)]. Discrete diffraction in the square lattice is observed at a bias field of  $900\ \text{V/cm}$  [Fig. 4.2(c)], clearly showing that most of the energy flows from the center towards the diagonal directions of the lattice. Even more importantly, a DS is observed at a bias field of  $3000\ \text{V/cm}$  [Fig. 4.2(d)], with most of energy concentrated in the center and the four neighboring sites along the principal axes of the lattice.

These experimental results are truly in agreement with expected behavior from the theory of discrete systems [54]. In fact, the above experimental observations are corroborated by our numerical simulations of the probe-lattice beam evolution equations using a fast Fourier transform multi-beam propagation method, in which the partially coherent lattice beam is described by

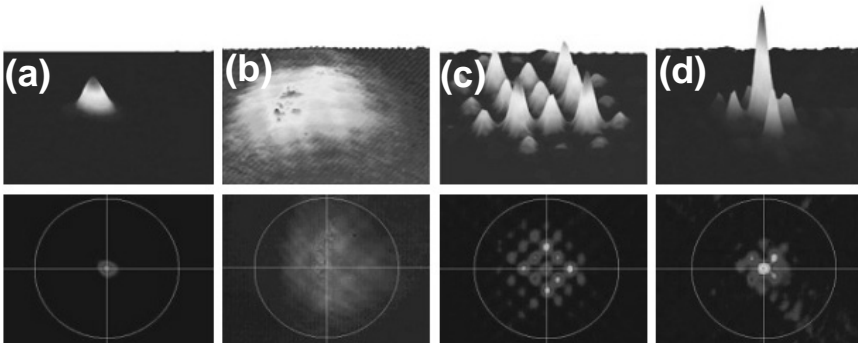


**Figure 4.2.** Experimental demonstration of a discrete soliton in a partially coherent lattice. (a) Input, (b) diffraction output without the lattice, (c) discrete diffraction at  $900\ \text{V/cm}$ , and (d) discrete soliton at  $3000\ \text{V/cm}$ . Top: 3D intensity plots; Bottom: 2D transverse patterns (after Ref. [10], and animation of the experimentally observed process can be viewed in Ref. [56]).

the so-called coherent density approach [55]. Typical numerical simulation results obtained with supercomputing time are shown in Fig. 4.3. The parameters chosen in simulation are close to those from the experiment. At a low bias field, discrete diffraction is observed (left), whereas at a high bias field the formation of a 2D discrete soliton is realized (right), in good agreement with experimental results. We point out that to form a 2D fundamental DS as shown in Fig. 4.2, a delicate balance has to be reached between waveguide coupling offered by the lattice and the self-focusing nonlinearity experienced by the probe beam through fine-tuning the parameters (the lattice spacing, the intensity ratio, the bias field, etc.). A series of experiments and numerical simulations were performed to show that large deviation in the beam intensities and/or the applied field (thus the strength of the nonlinearity) would hinder the DS formation [56].

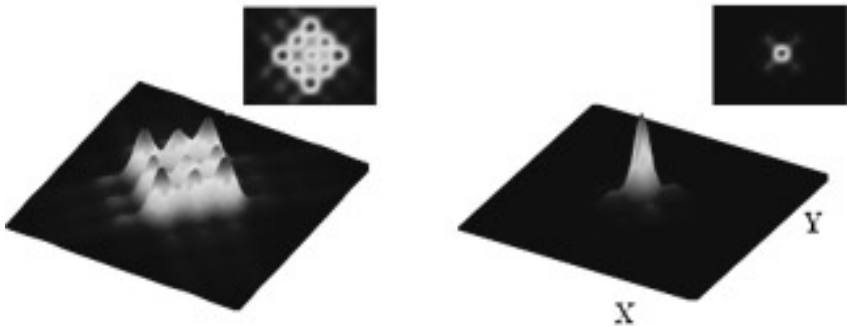


**Figure 4.3.** Numerical results corresponding to Fig. 4.2(c-d). Inserts are 2D transverse patterns.

## 6. Discrete vector and dipole solitons

The sensitivity of DS formation to the probe beam intensity not only illustrates that forming DS is the outcome of nonlinear self-action of the probe beam in the lattice, but also it can be used as a test bench for two-component vector-like DS [57-59]. While vector solitons have been realized previously in continuous nonlinear systems, they have been observed only very recently in a discrete system of 1D AlGaAs waveguide arrays [60]. Here we demonstrate that two mutually incoherent beams can lock into a 2D vector soliton while propagating along the same lattice site, although each beam alone would experience discrete diffraction under the same conditions. Typical experimental results of a 2D discrete vector soliton are presented in the first row of Fig. 4.4. The

two mutually incoherent beams (only one of them is shown in Fig. 4.4a) are launched into the same lattice site with combined peak intensity about 6 times weaker than that of the lattice beam. Discrete diffraction of each beam is observed at a low bias field of 1 kV/cm (Fig. 4.4b), but the two beams are coupled to form a discrete soliton pair at a high bias field of 2.9 kV/cm (Fig. 4.4c). The intensity patterns of each beam were taken immediately after blocking the pairing beam. In contrast, Figs. 4.4d shows that, after the pairing beam is removed and the remaining beam reaches a new steady state, each beam itself does not form a discrete soliton under the same conditions. These experimental results agree well with our numerical results shown in the bottom row of Fig. 4.4. Since the two components are exactly the same, only one of the components is shown. The exact solutions of such vector lattice solitons along with their stability regions have also been investigated [51].

Next, we demonstrate the formation of dipole solitons in a 2D optically induced photonic lattice by launching two mutually coherent beams into two neighboring lattice sites along the diagonal direction of the square lattice rather than overlapping them in the same lattice site. The two beams are made either out-of-phase or in-phase with each other, and we have found theoretically that both types of dipole-like solitons exist [52, 61]. The out-of-phase dipole solitons are linearly stable in a large range of parameter spaces with appropriate levels of nonlinearity, while the in-phase solitons are always linearly unstable although their instabilities are rather weak in the low-intensity regime [52, 61]. Experimentally, both types of lattice solitons are observed, but only the out-of-phase dipoles are found to be stable and robust under appropriate

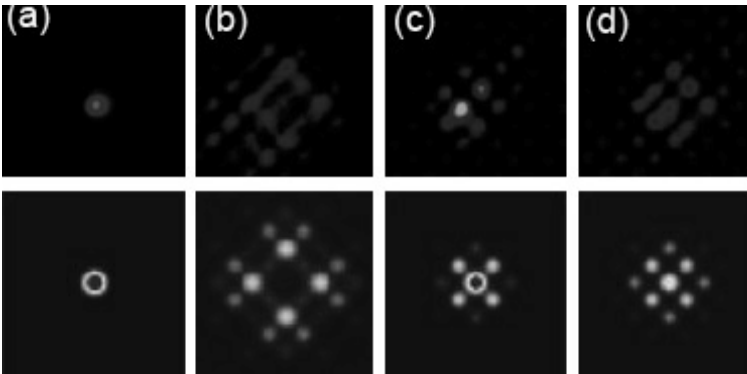


**Figure 4.4.** Experimental (top) and numerical (bottom) results of a 2D discrete vector soliton. (a) input, (b) discrete diffraction at low bias field, (c, d) mutual trapping and decoupled output at high bias field, respectively. Only one component is shown; the other component is the same or similar (after Ref. [51]).

conditions, while the in-phase dipoles suffer from instability as well as the anisotropic effect of the photorefractive nonlinearity [52, 61]. In the absence of the photonic lattice, these solitons cannot exist because of the repulsive or attractive force between the two humps which makes them diverge from or merge with each other. With the waveguide lattice, however, the lattice potential could trap the two humps against repulsion or attraction. These novel types of lattice solitons are related to the intrinsic localized modes found previously in 1D and 2D periodic nonlinear systems [62-64].

Typical results of the out-of-phase dipole lattice solitons are shown in Fig. 4.5. For the experiment, the dipole beams are oriented in the vertical direction (Fig. 4.5a), while the principal axes of the square lattice are oriented in diagonal directions. At a low bias field, the dipole undergoes linear discrete diffraction (Fig. 4.5b). At a high bias field, the dipole is trapped by the lattice potential, leading to the formation of dipole lattice solitons (Fig. 4.5c). Note that the initial phase structures are preserved after the lattice solitons are created, as seen from their output intensity patterns. Should one of the dipole beams be turned off, the other forms a fundamental lattice soliton and redistributes the energy to its center as well as four neighboring sites along the principal axes of the lattice in a manner similar to that in Fig. 4.2. Similar experiments have also been performed for the in-phase dipoles. A clear distinction between the two types of dipoles lies in the intensity redistribution

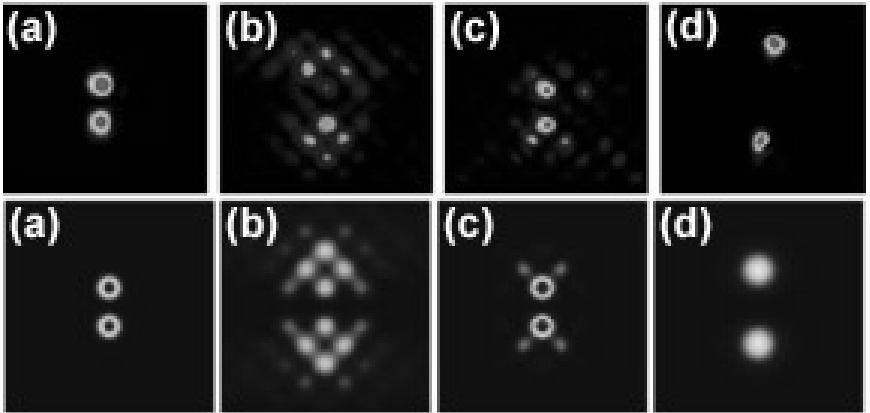


**Figure 4.5.** Formation of out-of-phase dipole solitons in a 2D photonic lattice for on-site probing with two mutually coherent beams. Top panel: experiment; bottom panel: numerical simulations. (a) input; (b) output at a low bias field of 100V/mm; (c) and (d) output at a high bias field of 320V/mm with and without the lattice, respectively. (after Ref. [52]).

after discrete diffraction at low bias fields: the intensity for the out-of-phase dipole extends along the original direction of the dipole, while that for the in-phase dipole extends along the orthogonal direction. However, at a high bias field, in-phase dipoles are also trapped by the lattice potential, leading to the formation of in-phase dipole solitons [61]. Without the lattice, the dipole diverges in the out-of-phase case (Fig. 4.5d) and merges into a single soliton in the in-phase case. Theoretically, we have simulated the evolution of out-of-phase dipole solitons, and the results are shown in the bottom panel of Fig.4.5. Qualitative agreement between numerical results and experimental observations is evident. In the experimental result of Fig. 4.5d, in addition to out-of-phase soliton repulsion, self-bending of the soliton elements towards crystalline  $c$ -axis (upward in Fig. 4.5d) is noticed. This soliton self-bending due to the diffusion effect enhanced by the high bias field is well known [65], so it has not been included in our theoretical model for simplicity. In addition to the dipole solitons presented above, we have also found other configurations of dipole-like solitons as well as quadrupole solitons in 2D lattices [61].

In addition to on-site excitation of the probe beams, we have also studied off-site excitations in weakly-coupled lattices created by optical induction. When a weak Gaussian-like probe beam (extraordinarily polarized, with a photo-sensitive wavelength such as 488 nm) is launched between two lattice sites, its energy switches mainly to the two closest waveguide channels evenly, leading to a symmetric beam profile. However, as the intensity of the probe beam exceeds a threshold value, the probe beam evolves into an asymmetric beam profile, akin to that resulting from the symmetry breaking in a double-well potential [66]. Should the probe beam itself experiences no or only weak nonlinearity (e.g., the probe is at a photo-insensitive wavelength such as 633 nm), such symmetry breaking in the beam profile does not occur regardless the increase of its intensity. When two probe beams are launched in parallel into two off-site locations, they form symmetric or anti-symmetric (dipole-like twisted [9, 52, 67]) soliton states depending on their relative phase as shown in Fig. 4.6. Keeping all other experimental conditions unchanged, we obtained quite different steady states between in-phase and out-of-phase excitations. In the in-phase case, most of the energy flows into the central lattice site [Fig. 4.6(a)], while in the out-of-phase case, the energy flows mainly into the two lateral sites in the vertical direction [Fig. 4.6(b)]. Radiation to other nearby lattice sites is also visible due to waveguide coupling. Intuitively, one may consider these new steady states as a result of constructive and destructive interference, but they correspond to symmetric (in-phase) and anti-symmetric (“twisted”) soliton states. The solitons are excited in an effectively three-well potential as embedded in a weakly coupled waveguide lattice. In fact, we have theoretically investigated this issue using a continuum model based on the saturable

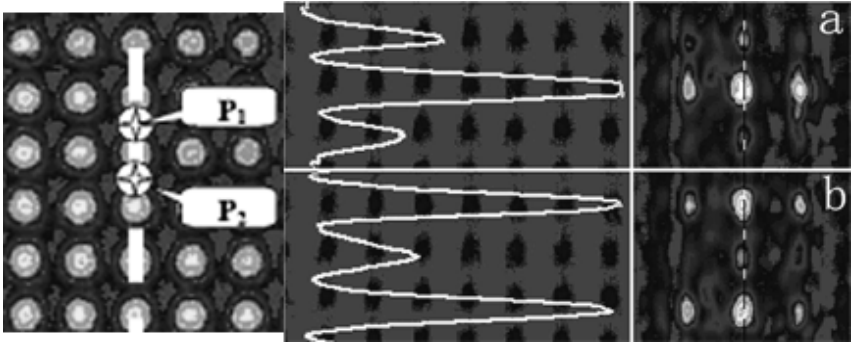


**Figure 4.6.** Formation of symmetric and anti-symmetric (twisted) soliton states for inter-site probing with two mutually coherent beams. Shown are the illustration of probe beam locations (P1 and P2) in the lattice (left), the combined output beam profile (middle), and the intensity pattern (right) for in-phase (a) and out-of-phase (b) excitations. (after Ref. [53])

photorefractive nonlinearity with an effectively three-well potential. We have found that in this setting any state with multiple in-phase beams (all centered on-site) is always unstable. However, both symmetric states (corresponding to a single beam on-site) and anti-symmetric states (corresponding to two out-of-phase beams on two different sites) can be linearly stable [53].

## 7. Discrete vortex solitons

An important nonlinear phenomenon in 2D lattices is the propagation of optical beams with complex internal structures in the lattice, e.g. the propagation of optical vortices carrying orbital angular momentum. Optical vortex solitons have been demonstrated earlier with continuous media in a number of experiments [68, 69], and the basic properties of vortices and vortex solitons can be found in a recent review article [70]. However, vortex solitons propagating in photonic lattices have not been demonstrated, even though they have been theoretically predicted [12, 13]. Here we present our experimental results of a vortex probe beam propagating in a 2D *linear* waveguide lattice. In this case, the lattice beam is *o*-polarized while the vortex beam is *e*-polarized. Typical experimental results on discrete trapping of the vortex with unit topological charge ( $m=1$ ) are shown in Fig. 4.7, for which a waveguide lattice with 28  $\mu\text{m}$  spacing is created. The vortex beam [normal diffraction shown in Fig. 4.7(a)] is then launched straight into the middle of the four lattice sites, so that the vortex center sits right in the middle of four lattice sites (off-site excitation [13, 14]). Due to waveguide coupling, the vortex beam undergoes discrete diffraction when

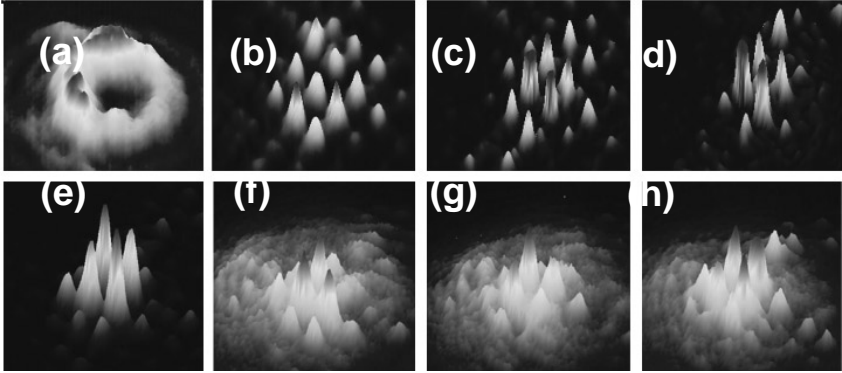


**Figure 4.7.** Formation of a singly-charged ( $m=1$ ) discrete vortex soliton in a 2D photonic lattice. Top panel shows the 3D intensity plots of the vortex beam at crystal output of normal diffraction without the lattice (a), output of discrete diffraction at low nonlinearity (b, c), and output of discrete soliton at high nonlinearity (bias field: 3000 V/cm). The lattice spacing is  $28 \mu\text{m}$ . Bottom panel shows discrete vortex soliton reproduced in a lattice of  $20 \mu\text{m}$  spacing (e), and a series of interferogram between the vortex soliton and a weak plane wave (f-h), confirming the nontrivial  $\pi/2$  step-phase structure of the vortex at different orientations. (after Ref. [14]).

the nonlinearity is low [Fig. 4.7(b-c)], but it evolves into a discrete vortex soliton at an appropriate level of high nonlinearity [Fig. 4.7(d)], with most of the energy concentrated at the central four sites along the principal axes of the lattice. To confirm the nontrivial phase of the vortex soliton, a weak reference beam is introduced to interfere with the discrete vortex after it exits the crystal. We use a piezo-transducer mirror in the reference beam path in order to control its phase relative to the vortex beam. As we actively move the PZT mirror, a series of interferogram is recorded to reconstruct the phase of the vortex. Examples of the interferograms are presented in Fig. 4.7(f-h), which shows that one of the four lobes increases its intensity whereas the corresponding diagonal lobe decreases its intensity. Furthermore, the lobe with the strongest intensity is alternating among the four spots. These interferograms confirm that the four lobes of the output vortex have a nontrivial phase relation --  $\{a \pi/2 \text{ phase ramp}\}$ , as expected for the discrete vortex soliton. Removing the reference beam, the discrete vortex soliton is restored in steady state [Fig. 4.7(e)].

In addition to self-trapping of vortices with unit topological charges ( $m=1$ ), we have also investigated the nonlinear propagation of high-order vortices in optically induced photonic lattices. Typical experimental results of discrete trapping of a doubly-charged ( $m=2$ ) vortex are presented in Fig. 4.8,



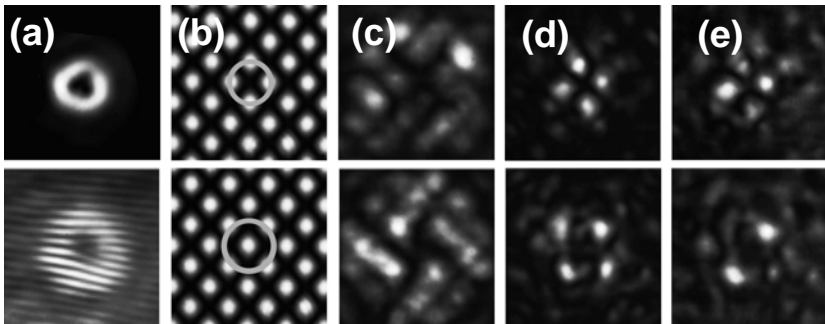


**Figure 4.8.** Formation of a doubly-charged ( $m=2$ ) discrete vortex soliton in a 2D photonic lattice with off-site (top) and on-site (bottom) excitations. (a) Input intensity pattern and interferogram of the vortex. (b) Lattice pattern with vortex input position marked by green circle. (c) Self-trapping of the vortex at bias field of 3.4 kV/cm. (d, e) Interference between (c) and a broad beam (quasi-plane wave) with two different phase delays, showing diagonal two spots are always in phase. (After ref. [71]).

where both on-site and off-site excitations with respect to the lattice orientation are illustrated [Fig. 4.8(b)]. The intensity pattern of the input vortex beam and its interferogram with a plane wave is shown in Fig. 4.8(a), confirming the double topological charges. Without bias field, the vortex breaks up into two singly-charged vortices during linear propagation. At a low bias field, the vortex undergoes discrete diffraction with its energy coupled to several lattice sites away from the vortex core, similar to that of Fig. 4.7(b) [71]. Self-trapping of the charge-2 vortex is achieved as the bias field is increased to above 2.0 kV/cm. The vortex breaks up primarily into 4 intensity spots as for the discrete singly-charged vortex soliton, but with major difference in the phase structure. For the singly-charged vortex soliton, it has been shown that the diagonal two spots are always *out of phase*. In fact, the relative phase among the 4 spots changes in steps of  $\pi/2$ , and such a step-phase structure is “frozen” during propagation [as shown in Fig. 4.7(f-h)], confirming a true vortex soliton [14, 15]. For the self-trapped doubly-charged vortex, similar experiment shows that the diagonal two spots are always *in phase* [Fig. 4.8(d, e)]. Furthermore, the interferograms show that the two spots in one diagonal are out-of-phase with the other two spots in the other diagonal for both on-site and off-site excitations. We note that, from Fig. 4.8(d) to Fig. 4.8(e), the relative phase between the vortex beam and the plane wave is changed by slightly moving a PZT mirror installed in the interferometer while keeping all other experimental conditions unchanged. (The background noise is mainly from the plane wave). From these measurements, it appears that the vortex beam breaks up into a quadrupole structure in lattices.

When the doubly-charged vortex breaks up into 4 spots in lattices, experimentally it is a challenge to distinguish between a true  $m=2$  vortex and a quadrupole soliton, although the issue has been investigated extensively in theory [72, 73]. The interferogram as in Fig. 4.8(d, e) would show similar results, while the interferogram as in Fig. 4.8(a) could not be obtained with good visibility due to weak central intensity and background noise. Fortunately, the vortex carries angular momentum while the quadrupole does not. Based on that, we examine the 4-spot pattern resulting from the vortex breakup at different level of nonlinearity. By changing the vortex-beam intensity or the bias field (both controls the photorefractive nonlinearity), we observe that the 4-spot pattern rotates slightly clockwise, and then reverses the direction of rotation to counterclockwise as the strength of the nonlinearity is increased. These observations suggest that the vortex beam should undergo a charge-flipping since the direction of rotation is related to the sign of the net topological charge [74, 75]. Such rotation and flipping is attributed to the nonlinearity-induced momentum exchange between the vortex and the lattice, which would not occur for a quadrupole lattice soliton without vorticity. Our numerical simulations show that the switching between clockwise ( $m=+2$ ) and anticlockwise ( $m=-2$ ) rotational modes of the vortex occurs periodically through a transition state, in which the vortex turns into a quadrupole-like structure with no phase variation across each intensity spot [71].

## 8. Discrete soliton trains and necklace-like solitons

As more complex soliton clusters in 2D lattices, we now report our work on formation of trains of 2D discrete solitons in a stripe shape as well as in a necklace shape. First, the DS trains in a row are generated by sending a stripe beam into a 2D square lattice [as the vertical stripe A in Fig. 4.1(b)]. When the lattice is operated in the linear regime, we observe that the stripe beam breaks up into 2D filaments, and then it evolves into a train of 2D discrete solitons as the level of the nonlinearity for the stripe is gradually increased. The first two photographs in Fig. 4.9 show the stripe beam at the crystal input [Fig. 4.9(a)] and its linear diffraction at the crystal output after 8 mm of propagation with the lattice absent [Fig. 4.9(b)]. The other photographs show the 2D discrete diffraction [Fig. 4.9 (c)] and the DS train formed at a bias field of 3.0 kV/cm [Fig. 4.9(d)] along with their corresponding 3D intensity patterns [Fig. 4.9(e, f)]. The observed behavior of the stripe beam in Fig. 4.9(c, e) arises clearly from discrete diffraction, in which most of the energy of the stripe beam goes away from the center (indicated by an arrow) to the two sides due to the waveguide coupling. When the self-focusing nonlinearity comes to play a role for the stripe beam at a new steady-state, the DS train is observed with most of energy being concentrated in the central column [Fig. 4.9(d, f)] to which the

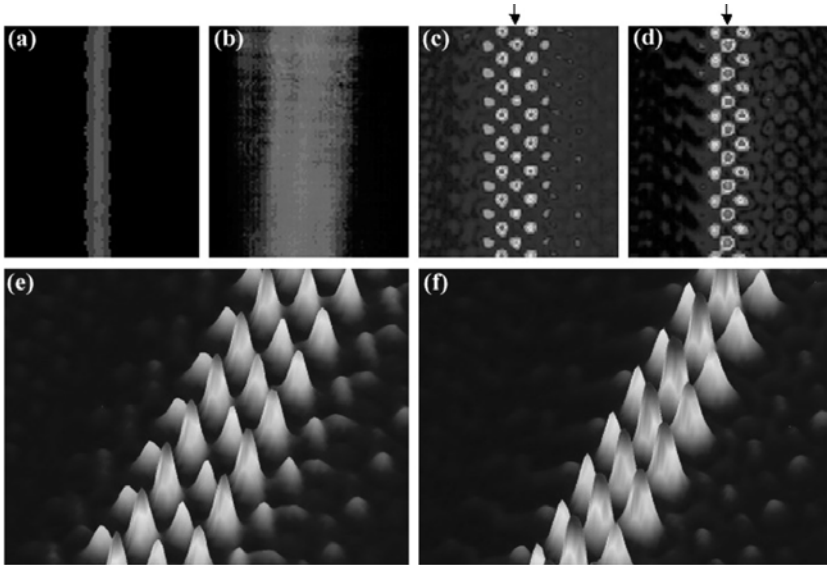


**Figure 4.9.** Experimental demonstration of 2D discrete soliton trains. Shown are the transverse intensity patterns of a stripe beam taken from crystal input (a) and output (b-d) faces. (b) Normal diffraction, (c) discrete diffraction, and (d) discrete soliton trains. Arrows in (c) and (d) indicate initial location of the stripe beam. (e) and (f) are 3D intensity plots corresponding to (c) and (d), respectively. (after Ref. [11]).

stripe beam was initially aimed. These experimental results are corroborated by numerical simulation of the stripe-lattice evolution equations using a fast Fourier transform multi-beam propagation method [10, 11]. The stability of such DS trains as well as the formation of DS trains in other configurations such as a necklace-like ring discrete solitons discussed below certainly merits further investigation. We note that the formation of soliton trains mediated from modulation instability is a fundamental nonlinear wave problem as discussed recently also with coherent matter waves [76, 77].

Next, we present the results on the DS trains in a necklace shape which are generated by sending a high-order vortex ( $m=4$ ) beam into a 2D square lattice [as illustrated in Fig. 4.10(a)]. Our experiments were performed in a 2D square lattice optically induced by passing a laser beam (with wavelength 488 nm) through a rotating diffuser, an amplitude mask, and a biased PR crystal, as described earlier. The biased crystal (20 mm long SBN:60) provides a self-focusing noninstantaneous nonlinearity. Because of the anisotropic property of the PR crystal, the ordinarily polarized lattice beam experiences only a weak nonlinearity and forms a stable 2D waveguide array nearly invariant during

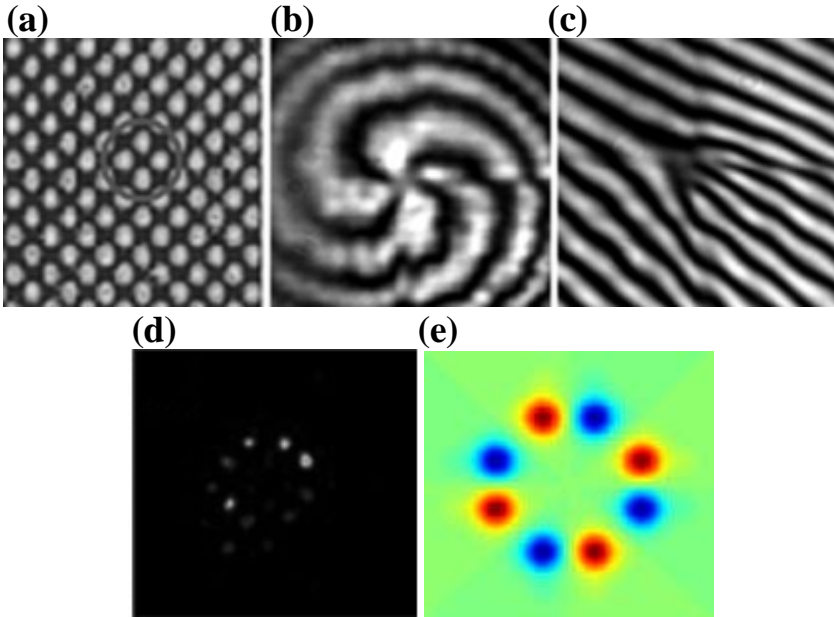


**Figure 4.10.** Formation of a necklace-like soliton in a 2D photonic lattice. (a) a 2D photonic lattice created by optical induction, where the circle indicates the off-site vortex location. (b, c) the interferograms of a charge-4 vortex with a spherical and a plane wave, respectively. (d) experimental observation of the self-trapped vortex into a necklace shape. (e) the electric field distribution of a necklace soliton as obtained from theory, where the red and blue spots have  $\pi$  phase difference between adjacent pearls. (after Ref [78]).

propagation in the crystal. The principal axes of the square lattice are again oriented in the diagonal directions. To facilitate the formation of a necklacelike soliton, a ring vortex beam is launched into the lattice such that the ring covers 8 lattice sites, with the center of the ring located in an empty site (off site) as shown in Fig. 4.10(a). The ring vortex is created with a charge-4 ( $m=4$ ) helicoidal phase mask, and the phase singularity of the vortex is shown in the interferograms of Figs. 4.10(b, c). The vortex beam is coherent (without going through the diffuser) and extraordinarily polarized. Thus, it experiences a much higher nonlinearity while propagating collinearly with the lattice beam through the biased crystal. Typical experimental observation of self-trapping of the high-order vortex is presented in Fig. 4.10(d). To achieve self-trapping, a stable square lattice (with  $40 \mu\text{m}$  lattice spacing) is created in the crystal first. A vortex beam with charge-4 and intensity about 5 times weaker than that of

the lattice is then launched into the lattice, with the vortex ring covering 8 sites in a necklace or octagon shape. The vortex beam exhibits significant diffraction after linear propagation through the crystal. Without the lattice, the charge-4 vortex breaks up into many filaments in the self-focusing nonlinear crystal, leading to disordered patterns driven by noise and modulation instability [78]. In the presence of the lattice, however, the behavior of the vortex is dramatically different, characterized by the confinement of the filaments at about the location of the initial vortex ring. This is shown in Fig. 4.10(d), where the vortex has evolved into an octagon (necklace-like) structure at an appropriate level of high nonlinearity. Such a soliton cluster is stationary and quite stable during the period of observation (typically more than 30 min), so the soliton structure is observed in steady state. This structure is due to the nonlinear self-action of the vortex-ring beam. When the center of the initial vortex ring is moved from the off-site position to an on-site one, the octagon structure disappears. But when the vortex ring is lined up again with 8 octagon-shaped lattice sites (at a different off-site location), the necklace structure is restored in a new steady state [78]. Thus the offsite excitation favors the formation of the necklace soliton. The experiment was repeated with vortices of different topological charges. When a ring vortex beam with charge lower than 4 is launched into the same octagon-shaped lattice sites, less confined necklace structures are observed. Even for the case of a charge-4 vortex where the robust necklace structure is observed, we could not achieve sufficiently high visibility to determine the entire phase structure of the necklace soliton by the interference technique, as was done for lower-order vortex solitons described earlier. This is simply due to the imperfection of the vortex mask that results in unequal intensities for the pearls in the necklace and the strong sensitivity to the background noise. The above experimental results were corroborated by our theoretical studies through two different (yet complementary) approaches; one is to use the continuous model with a periodic lattice potential, and the other is to use the discrete nonlinear Schrodinger equation [78]. Both approaches revealed existence of such necklace solitons. Furthermore, it has been shown that stable necklace-like solitons can only be obtained when the adjacent pearls in a necklace are out-of-phase rather than in-phase, as shown in Fig. 4.10(e).

## 9. “Fabrication” of 2D ring lattices and nonlinear discrete trapping

Although discrete solitons have been demonstrated experimentally in a variety of settings, including semiconductor waveguide arrays with Kerr nonlinearity [4, 5], optically-induced waveguide lattices with photorefractive nonlinearity [7-11], fabricated channel waveguides in lithium niobate crystals

with quadratic nonlinearity [79], and voltage-controlled waveguide arrays in liquid crystals with orientational nonlinearity [80], all the experimental work on discrete solitons has been performed either in 1D lattices or in 2D lattices with no rotational symmetry (e.g., planar or square lattices). On the other hand, in the 2D domain, many fundamental features are expected to occur not only because lattice structures can be richly configured with different lattice symmetry, but even in a given lattice symmetry (such as in square lattices), spatial solitons that have no analog in the 1D domain can be realized. When the rotational symmetry is desired, one can have another important class of lattices such as those created by nondiffracting Bessel beams [81]. Such lattice symmetry may lead to new soliton features attractive for applications in soliton manipulation including the possibility to induce rotary soliton motions and reconfigurable soliton networks [82].

Motivated by this, we demonstrate for the first time the formation of Bessel-like photonic lattices by optical induction. Such ring-shaped lattices remain nearly invariant in a 10-mm long photorefractive nonlinear crystal. Different from what was used earlier for generation of soliton pixels [35] and DS in square lattices [10, 11, 14], here we use an amplitude mask with an equally-spaced concentric ring pattern. A coherent laser beam operating at 532-nm wavelength is split into two beams by a polarizing beamsplitter (PBS) before entering into a 10-mm long SBN:60 photorefractive crystal. The lattice-forming beam passing through the mask is ordinarily-polarized (*o*-beam), and the soliton-forming beam is extraordinarily-polarized (*e*-beam). When the mask is imaged onto the input face of the crystal, a spatial bandpass filter is introduced in the Fourier plane. After proper filtering, the mask gives rise to a Bessel-like intensity pattern at the crystal input [Fig. 5.1, left panel], which remains nearly invariant during linear propagation. We note that the ring pattern created this way is slightly different from the true Bessel pattern, since both the intensity and the spacing between adjacent rings do not decrease so dramatically in the radial direction. (In fact, the true Bessel pattern has a normalized intensity of 1.00, 0.16, 0.09 and 0.06 for the first four maxima, while our measured normalized intensity is 1.00, 0.25, 0.14, and 0.10. Starting from the first ring, the measured spacing between adjacent rings is about 20  $\mu\text{m}$  even far away from the center). With an appropriate bias field, such a ring pattern from *o*-beam induces a periodic ring waveguide lattice that propagates nearly linearly throughout the 10-m long crystal. To fine-tune the lattice potential and the nonlinearity of the probe beam, a background illumination from an incandescent lamp is used to cover the entire crystal from the top.

Discrete diffraction and discrete solitons are observed when a probe beam is launched both into the lattice center and into different lattice rings. In the former

case (center excitation), we demonstrate a clear transition from discrete diffraction to linear single-channel guidance by fine-tuning the lattice potential and to nonlinear self-trapping of the probe beam by fine-tuning the self-focusing nonlinearity. In the latter case (off-center excitation), we also demonstrate controlled soliton rotation in different lattice rings by imposing an initial transverse momentum to the soliton. To ensure trapping of the probe beam results from nonlinear self-action rather than simple guidance, we take advantage of noninstantaneous nature of the photorefractive nonlinearity. Experimental results are illustrated in Fig. 5.1, where (a, c) show the linear diffraction patterns which were taken 0.05 s after the probe beam ( $11.5\mu\text{m}$ , FWHM) was launched into the lattice (before self-action took place), and (b, d) shows the corresponding self-trapped patterns taken 60 s later when the crystal has reached a new steady-state. For on-center excitation [Fig. 5.1, top], the peak intensity ratio between the central core of the lattice and the probe beam is about 1:4, and the applied dc field is 3.00 kV/cm. For off-center excitation [Fig. 5.1, bottom] where the probe is aimed at the third ring, the intensity ratio between the third lattice ring and the probe beam is about 1:8, and the applied field is 3.80 kV/cm. As seen from these figures, the probe beam undergoes strong discrete diffraction before nonlinear self-action takes place, with the diffracted beam covering several lattice rings, but its energy becomes much more localized due to nonlinear self-trapping. We emphasize that the results in Fig. 5.1 are from the *nonlinear* self-action of the beam in the lattice, which is different from *linear* guidance of light by a high-index core as in an optical fiber.

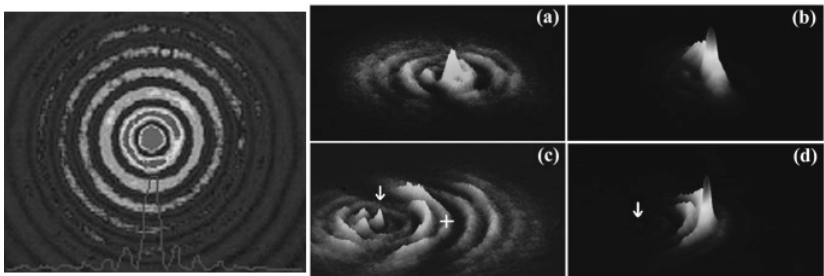


**Figure 5.1.** Left panel: Optically induced Bessel-like ring lattices in a self-focusing medium. Right panels: Transition from discrete diffraction (a, c) to nonlinear self-trapping (b, d) of a probe beam launched in the center (a, b) and the third ring (c, d) of the lattice. Patterns in (a, c) were taken instantaneously ( $<0.1$  s) while those in (b, d) were taken in steady state. The arrow indicates the center of the ring lattice, and the cross indicates the input position of the probe beam. (after Ref. [83]).

A fascinating property of solitons particular to the setting of ring lattices is that such solitons can rotate around the rings without much radiation during their rotary motion [81]. To demonstrate such soliton rotation experimentally, we launch the probe beam on the far right side of the ring with a tilting angle towards the  $y$ -direction, thus imposing an initial transverse momentum to the probe. We observe that the degree of soliton rotation increases with the tilting angle for the same ring excitation, but decreases as the soliton is created at the larger rings. Figure 5.2 shows the rotary motion of the soliton in different rings with the same tilting angle (top panel), and in the same ring with different tilting angles (bottom panel). For these experimental results, the space between the rings is about  $40\mu\text{m}$ , the intensity ratio between the ring which the soliton locates and the peak of the probe beam is about 4:9, and the applied dc field is  $5.2\text{ kV/cm}$ . From Fig. 5.2, we see clearly that the probe beam with a tilting angle can form a spatial soliton that rotates along the ring it is created. Furthermore, with the same tilting angle, the rotary angle decreases as the soliton is excited in the outer rings, as expected from particle rotation. Our experimental results are in good agreement with the theoretical analysis of these effects [83]. These rotary solitons are expected to play new roles in soliton-driven photonics, and their experimental realization might provide insights for studying similar phenomena in other nonlinear systems of periodic ring structures.

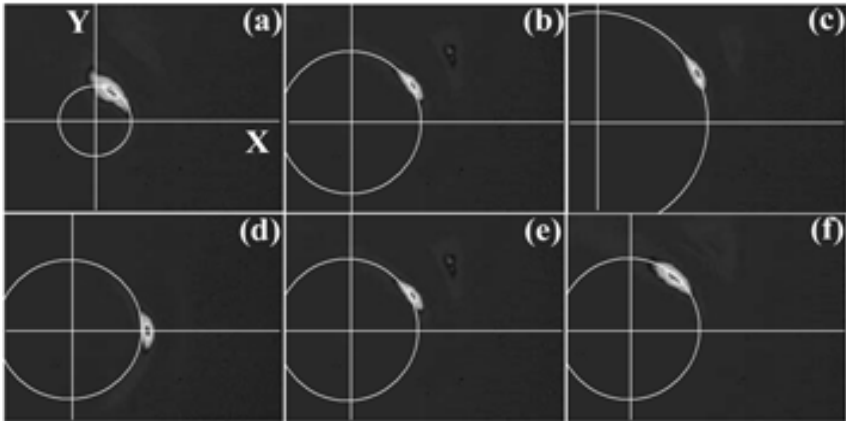


**Figure 5.2.** Soliton rotation in optically-induced ring lattices. From (a) to (c), the probe was aimed at the far right side of the first, second and third ring with the same tilting angle (about 0.4 degree) in  $y$ -direction. From (d) to (f), the probe was aimed at the same second ring but with different tilting angles of 0, 0.4 and 0.6 degree, respectively.



It should be pointed out that all work presented in Sect. 4 and Sect. 5 is about discrete solitons in 2D *linear* waveguide lattices where the probe beam experiences a strong self-focusing nonlinearity but the lattice beam does not. Discrete solitons are so called because a delicate balance between self-focusing from nonlinearity and discrete diffraction from lattices has been reached for each of these self-trapped states, so that the wavepackets could propagate invariantly through the periodic medium. On the other hand, such balance may not be reached should the lattice beam itself experiences strong nonlinearity. In this latter case, however, it is possible to demonstrate a number of novel phenomena associated with soliton-lattice and vortex-lattice interactions, including soliton-induced lattice dislocation, lattice deformation and compression, and vortex-induced lattice twisting due to the transfer of angular momentum carried by the vortex into a nonlinear solitonic lattice. Part of the work with *nonlinear* solitonic lattices are reviewed in Ref. [50]. For discrete solitons in linear lattices, only the probe beam experiences high nonlinearity. For soliton-lattice interaction, both the probe beam and the lattice beam experience high nonlinearity. In what follows (Sect 6. and Sect 7), we shall discuss light confinement by defects embedded in otherwise uniform lattices, in which both the probe beam and the lattice beam experience no or only weak nonlinearity.

## 10. “Fabrication” of 2D defective square lattices and linear bandgap guidance

Periodic lattices with impurities and defects are well known in solid state physics, photonic crystals and fabricated semiconductor waveguide arrays. In particular, bandgap guidance by defects in otherwise uniformly periodic structures such as hollow-core photonic crystal fibers (PCF) is fundamentally different from traditional guidance by total internal reflections (TIR). As mentioned earlier, such PBG has been demonstrated earlier in 2D arrays of dielectric cylinders with isolated defects for microwaves, and recently in all-solid PCF with a lower-index core for optical waves.

In photonic lattices optically-induced in a photorefractive crystal [6-11], the induced refractive index variation is typically orders of magnitude smaller than that in photonic crystals, while the lattice spacing is also much larger than the optical wavelength. A natural question arises: is it possible to optically induce 2D waveguide lattices with a single-site defect so that light can be confined in the defect akin to those achieved in hollow-core PCF? That would open up another avenue for studying the defect-related phenomena in periodic systems, taking advantage of the unusual features of photorefractive materials such as wavelength-sensitive and reconfigurable nonlinear refractive index patterns induced at very low power levels.

Here we report the first experimental demonstration of PBG in optically-induced 2D photonic lattices with a single-site negative defect [31]. In such a defective lattice, the refractive index in the defect is lower than that in the surrounding “rods” (akin to an “air defect” in photonic crystals or hollow-core PCF [16, 17], and much alike all-solid low-index-core PCF [19, 20]). We observe that a probe beam at different wavelengths is spatially confined in the defect during its linear propagation, although the defect is repulsive and the beam itself has no nonlinear self-action. The observed “guidance” of light in the negative defect arises from linear propagation of the DM formed in the spatial bandgap of the photonic lattice, which is fundamentally different from linear guidance by TIR or nonlinear self-guidance as in a spatial soliton. In addition, we show that the “guided” patterns by the defect display fine spatial structures such as dipole and vortex cells which arise from the DM excited at higher bandgaps.

Using experimental techniques similar to those for 1D defective lattices, we can optically generate 2D square defective lattices as well. As before, we not only need to employ frequency filtering and beam tilting to eliminate the Talbot effect, but also need to introduce weak nonlinearity and partial incoherence to maintain the defect against washing-out. The experimental results are shown in Fig. 6.1 (top panel). Here Fig. 6.1 (a) is the lattice input, with lattice spacing about  $27\mu\text{m}$ . The propagation distance is 20mm. In purely linear propagation, the defect disappears at the exit face of the crystal [see Fig. 6.1(b)]. However, when weak nonlinearity is introduced to the lattice beam, the defect is well maintained [see Fig. 6.1(c)]. The 2D defect can guide 2D localized modes as well, similar to the 1D case. To demonstrate, we experimentally launch a weak probe beam into the defect nested in the otherwise uniform lattice as shown in Fig. 6.1 (bottom panel). The input of the probe beam is shown in Fig. 6.1(a). When the defect is not maintained as in (b), the probe beam strongly diffracts (see bottom (b)). However, when the defect is well maintained, the probe beam is very well guided inside the defect (see bottom (c)). It is important to point out that, should the lattice be removed, the probe beam itself has no (or very weak) self-action so that it diffracts normally. Since the probe beam is guided by the defect where the refractive index is lower compared to its surroundings (negative defect), total internal reflection does not occur here.

One of the interesting phenomena in 2D defect guiding is the observation of fine structures in the “tails” of DM patterns, which has no counterpart in 1D defect guiding. These fine structures appear at different lattice conditions. In Fig.6.2, three such characteristic patterns are presented. At lattice spacing of  $27\mu\text{m}$ , the “tails” resulting from the leakage of light extend afar from the center core and cover more than just a single diagonal line of the lattice (Fig. 6.2(a)).

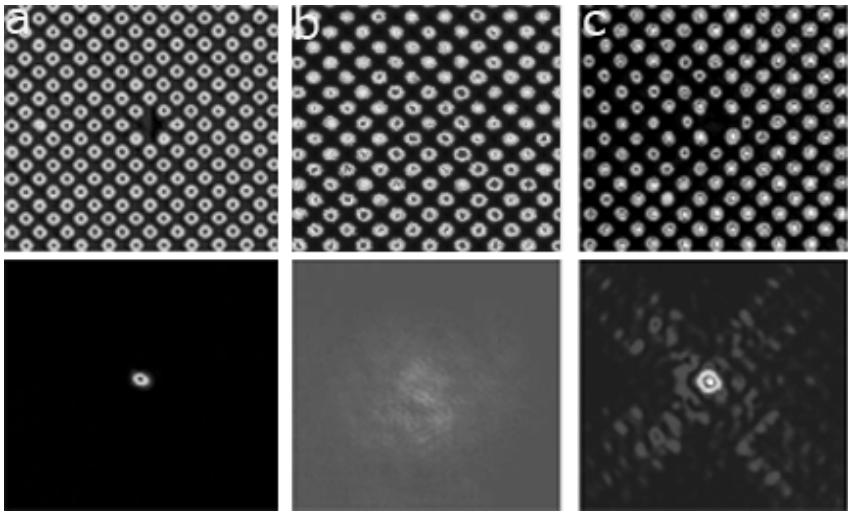


**Figure 6.1.** Top panel: intensity pattern of a 2D induced lattice with a single-site negative defect at crystal input (a) and output (b, c). The defect disappears in linear region (b) but can survive with nonlinearity (c) after propagating through 20-mm long crystal. Bottom panel: input (a) and output (b, c) of a probe beam showing normal diffraction without the lattice (b) and bandgap guidance by the defect (c) under the same bias condition. (after Ref. [31]).

At spacing  $42 \mu\text{m}$ , the “tails” in the output patterns display even more interesting fine structures associated with non-trivial phase distributions (Fig. 6.2 (b, c)). Such phase pattern was recorded by the interference between the probe beam forming the DM and a broad beam (quasi-plane wave). It revealed that the “tails” along the lattice principal axes contain either dipole-like (Fig. 6.2 (b)) or vortex-like (Fig. 6.2 (c)) arrays. Figure 6.2 (d) shows a typical interferogram corresponding to intensity pattern of Fig. 6.2 (c), where the locations of vortices are indicated by arrows. It is apparent that the vortex cells have different sign of topological charge in two diagonal “tails”.

To theoretically understand these various patterns of 2D defect-mode structures, we use the 2D model equation

$$iU_z + U_{xx} + U_{yy} - \frac{E_0}{1 + I_L(x, y)} U = 0, \quad (6.1)$$

where  $U$  is the envelope function of the probe beam,  $E_0$  is the applied bias field,

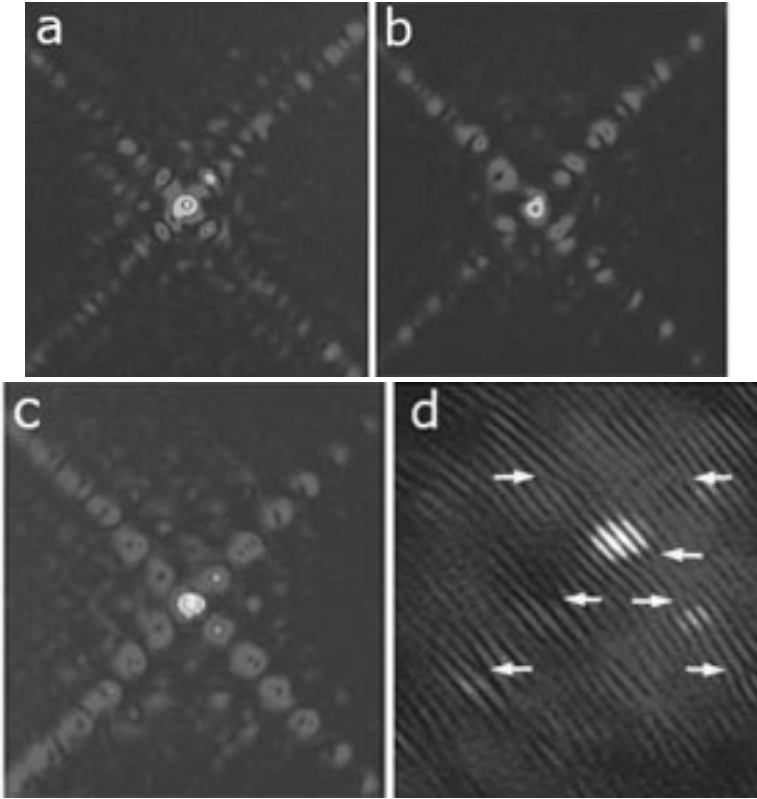


**Figure 6.2.** Intensity patterns of DM under different lattice conditions. (a) lattice spacing  $27 \mu\text{m}$ , bias field  $E= 2.6 \text{ kV/cm}$ ; (b) lattice spacing  $42 \mu\text{m}$ ,  $E= 2.4 \text{ kV/cm}$ ; (c) lattice spacing  $42 \mu\text{m}$ ,  $E= 3.0 \text{ kV/cm}$ . (d) zoom-in interferogram of (c) with a plane wave where arrows indicate location of vortices. The brightest spot corresponds to the defect site (after Ref. [31]).

$$I_L(x, y) = I_0 \cos^2\left(\frac{x+y}{\sqrt{2}}\right) \cos^2\left(\frac{x-y}{\sqrt{2}}\right) \left[1 - \varepsilon \exp\left(-\frac{(x^2+y^2)^4}{128}\right)\right] \quad (6.2)$$

is the 2D defective lattice,  $I_0$  is the lattice peak intensity, and  $\varepsilon$  is the defect depth. When we take  $E_0 = 12$ ,  $I_0 = 3$ , and  $\varepsilon = 0.1$ , we find various 2D defect modes which are shown in Fig. 6.3. In this figure, (a) shows the bandgap structure of this 2D lattice system. At point B which lies in the first bandgap (between the two lowest Bloch bands), there is a single defect mode shown in (b). This mode is symmetric along the two lattice principal axes, and it closely

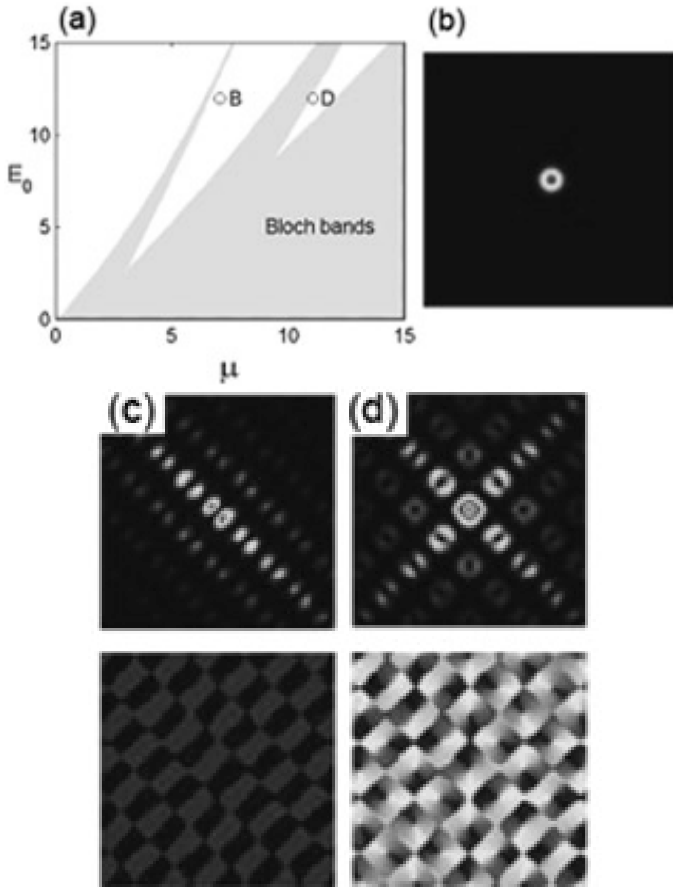


**Figure 6.3.** (a) Bandgap structure of a 2D uniform lattice ( $I_0 = 3$ ); (b) a defect mode found at point B in (a); (c) another defect mode  $\psi(x,y)$  found at point D in (a); (d) a linear superposition of defect modes  $\psi(x,y)$  and  $\psi(y,x)$  with a  $\pi/2$ -phase delay. Upper panel shows intensity patterns and lower panel the phase plots (after Ref. [31]).

resembles the one observed in Fig. 6.1(a) and 6.2(a). However, at point D, which lies in the second bandgap, we find two defect modes  $\psi(x,y)$  and  $\psi(y,x)$  which are asymmetric along the two lattice principal axes. One of these two modes is shown in Fig. 6.3(c), while the other one is a 90-degree rotation of Fig. 6.3(c). Due to the linear nature of this system, any linear superposition of these two defect modes remains a defect mode. Depending on the relative

phase between these two modes, their linear superposition can give rise to very interesting mode patterns. For instance, when these two modes have a 90-degree phase delay, their superposition  $\psi(x, y) + i\psi(y, x)$  is shown in Fig. 6.3 (d). It is seen that this new defect mode contains an array of vortex cells, dominated along the two lattice principal axes. This pattern is quite similar to the one observed in Fig. 6.2 (c, d). The dipole arrays observed in Fig. 6.2 (b) may be explained in a similar way. These experimental and theoretical findings reveal that light guiding behaviors by 2D defects are much richer and merit further study.

## 11. “Fabrication” of 2D ring lattices with a low-index core and its linear guidance

As discussed in previous sections, recent work has predicted the possibility of spatial confinement of light (defect modes) in optically-induced waveguide lattices with local defects. Indeed, such defect modes have been observed in both 1D stripe and 2D square lattices with a single-site defect. However, it remains a challenge to optically induce a PCF-like lattice structure with a negative defect (a low-index core) to demonstrate PBG guidance. Although in the nonlinear region a light beam itself can induce a defect via nonlinearity in waveguide lattices, and thereby localize itself in the induced defect such as “discrete solitons” [1-15], these localizations via nonlinear self-action are fundamentally different from the PBG guidance in which a light beam itself undergoes linear propagation.

In this section, we present the results on the formation of Bessel-like photonic lattices by optical induction in a *self-defocusing* photorefractive crystal, as well as the light guiding property in such lattices [30]. When propagating through the crystal, a spatially modulated lattice beam induces a set of concentric rings of index change with a low index core. Such index structure is similar to those of Bragg fiber and Omniguide fiber, but it is reconfigurable with low index change on the order of  $10^{-3}$  to  $10^{-4}$  and the lattice period (“pitch”) on the order of tens of microns. A transition of probe beam from linear discrete diffraction to the guidance into the low-index core is clearly observed by fine-tuning the lattice potential. We show theoretically that this guidance persists when the outer rings of the lattice are removed, and discuss the possible mechanism for the observed guidance in experiment.

The crystal used in our experiment is a 10-mm long SBN:61. The experiment setup is similar to that used for generation of discrete ring lattice solitons reported in Sect. 5, except that the Bessel-like lattices are induced with a *self-defocusing* nonlinearity, so the center of the lattice is a low index core. With proper filtering, the mask gives rise to a Bessel-like intensity pattern at the crystal input [Fig. 7.1(a)], which remains nearly invariant during the propagation

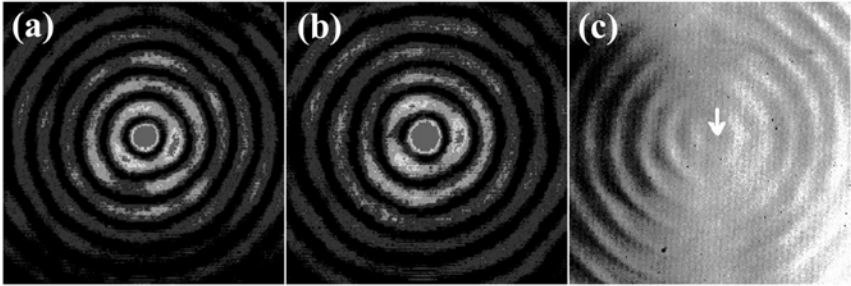


**Figure 7.1.** Intensity pattern of a ring lattice at crystal input (a) and output (b) after 10-mm of propagation. (c) A broad incoherent beam probing through the lattice shows a reversed contrast respective to (b). The arrow in (c) marks the center of the lattice (i.e., the low-index core). (after Ref. [30]).

throughout the 10-mm long crystal even under a negative bias field of 2 kV/cm [Fig. 7.1 (b)]. Starting from the first ring, the measured spacing between adjacent rings in Fig. 7 is about  $20 \mu\text{m}$ . We note that the ring pattern created this way is somewhat different from the true Bessel pattern, since the intensity of rings does not decrease as dramatically in the radial direction as in a true Bessel pattern. With a *negative* bias, the crystal has a *self-defocusing* nonlinearity [36, 45, 46]. This means that the locations of the ring waveguides correspond to the dark (low intensity) areas of the lattice beam, while the center (high-intensity) corresponds to an anti-guide. Thus the ring pattern in Fig. 7.1(b) induces a periodic ring waveguide lattice with a low-index core, tested by sending a broad white-light probe beam as shown in Fig. 7.1(c). The guided pattern of the probe beam has a reversed contrast as compared to the intensity pattern of the lattice beam.

To investigate the waveguiding property in such an induced ring lattice, a Gaussian-like probe beam (FWHM:  $14 \mu\text{m}$ ) is launched directly into the core and propagate collinearly with the lattice. The probe beam is *e*-polarized but has a wavelength of 632.8 nm that is nearly photo-insensitive for our crystal, so that nonlinear self-action of the probe beam is negligible. Since the index at the center of the lattice is lower than that at its surrounding, the probe beam tends to escape from the center and couple into the surrounding ring waveguides due to evanescent coupling. As such, the peak intensity of the probe beam does not stay in the core after linear propagation and discrete diffraction. However, under appropriate conditions, guiding of the probe beam into the core is observed. Typical experimental results are presented in Fig. 7.2 for a ring lattice with the spacing of  $37 \mu\text{m}$ . Figure 7.2 shows the output patterns

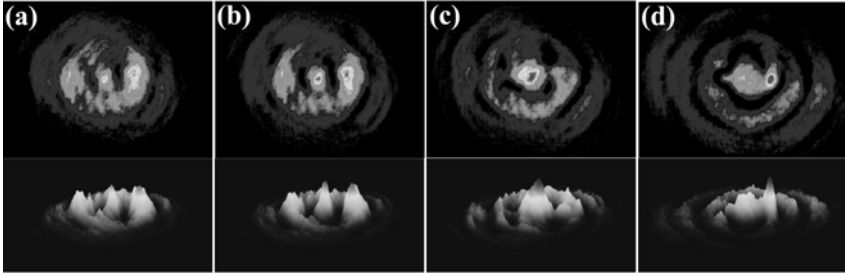


**Figure 7.2.** Propagation of the probe beam in the ring lattice. (a-d) 2D output transverse patterns (top) and corresponding 3D intensity plots (bottom) of the probe at a fixed lattice intensity while the negative bias is increased gradually (0.6, 1.0, 1.4, and 2.0 kV/cm) (after Ref. [30]).

of the probe beam as the applied dc field is set at different levels while the lattice intensity (normalized to background illumination) is fixed. When the bias field is low, the probe beam tends to diffract away from the core [Fig. 7.2 (a)], but as the bias field increases, the probe beam undergoes a transition from discrete diffraction to central guidance [Fig. 7.2 (c)]. This phenomenon resembles that reported for 1D and 2D defect modes presented earlier. At even higher bias field, the guidance starts to deteriorate [Fig. 7.2 (d)] because the experimental condition deviates from that for the formation of the defect mode.

We emphasize that in these experiments the probe beam has no self-action because of its photo-insensitive wavelength. Should the probe beam be at a photo-sensitive wavelength (e.g., 488 nm), it would experience the *self-defocusing* nonlinearity which in turn would make the beam spread more. If a positive bias is used to turn the crystal into a *self-focusing* medium, the induced ring lattice will have a high-index core, where a probe beam can be either guided (by total internal reflection) or self-trapped to form a discrete soliton. Since our observed guidance differs from total internal reflection and nonlinear self-induced waveguiding, its mechanism merits further investigation.

To better understand the experimental results in Fig. 7.2, we use the model equation  $iU_z + U_{xx} + U_{yy} - \frac{E_0}{1 + I_0 |J_0(r)|^{3/2}} U = 0$ , where  $J_0(r)$  is the Bessel function,

and  $r = \sqrt{x^2 + y^2}$ . Here  $x$  and  $y$  are normalized by the spacing (pitch) of the lattice far away from the center, and normalizations for  $I_0$ ,  $E_0$  and  $z$  are the same as in [30]. The Bessel function  $|J_0(r)|^{3/2}$  was chosen for the ring lattice since the first four peaks of this function decay as 1.00, 0.25, 0.16, 0.12 [Fig. 7.3(a)], closely resembling those in the experiments. Numerical simulations under experimental conditions produce results qualitatively similar to those in



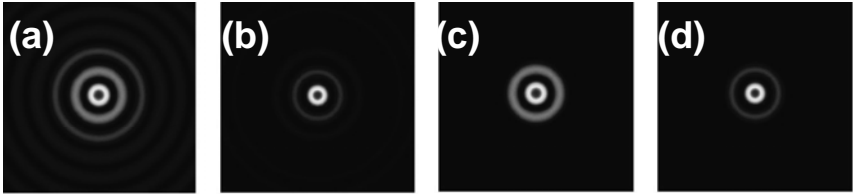


**Figure 7.3.** Ring waveguides and their quasi-localized modes. (a) A Bessel-like ring lattice; (b) a guided mode in (a); (c) the lattice of (a) with outer rings removed; (d) a guided mode in (c). Normalized parameters are  $E_0 = -15$ ,  $I_0 = 750$ , and  $\mu = 0.97$  ( $E_0 = -15$  corresponds to  $-1.4$  kV/cm).

Fig. 7.2. Furthermore, we have also searched for guided modes of the above model in the form of  $U(x, y, x) = e^{-i\mu z}u(r)$ , and found solutions  $u(r)$  which have a high central peak and weak oscillatory tails. One such solution is shown in Fig. 7.3(b), which resembles those observed in Fig. 7.2(c). The amplitudes of the tails in such solutions depend on  $E_0$ ,  $I_0$  and  $\mu$ . Note that in our ring lattice, the intensity decays along the radial direction, and thus bandgaps do not really open in the above model. Thus, the solution in Fig. 7.3(b) can not be a truly localized defect mode. If we keep only the central beam and the first ring of the lattice [see Fig. 7.3(c)], we find that quasi-localized modes as in Fig. 7.3(b) persist [see Fig. 7.3(d)]. This finding indicates that the guidance observed above may not be attributed to the repeated Bragg reflections of outer rings, but rather it is dominated by the first high-index ring in our lattice. This guidance seems analogous to that in antiresonant reflecting optical waveguides [84], and certainly merit further investigation. For instance, one of the subjects in our future research is to see if such low-index core can create any “coloring” effect as that occurred in photonic crystal fibers.

## 12 . Summary

In summary, we have successfully fabricated, or optically induced, 1D and 2D uniform and defective photonic lattices by the method of amplitude modulation together with several other techniques such as frequency filtering, partial spatial coherence, and polarization-controlled index variation. These lattices can propagate in linear, weakly nonlinear and strongly nonlinear regimes. We have also demonstrated that these lattices can support linear and nonlinear localized states of beam propagation with various geometrical and phase structures, such as dipole solitons, vortex solitons, necklace-like solitons, linear defect modes, and bandgap guidance akin to that occurs in photonic crystals. The mechanisms for light confinement in these lattice

structures range from nonlinear discrete self-trapping, repeated Bragg reflections, and the anti-resonance effect. Our results pave the way for further study of new phenomena in periodic and irregular photonic structures, as well as for exploring potential applications in beam shaping and light routing with reconfigurable lattices.

We close by mentioning that, in this Chapter, we have provided an overview mainly about our own work on optically-induced photonic lattices and their linear and nonlinear light guiding properties. There are a number of research groups worldwide actively working in this dynamically changing field of nonlinear optics and photonics [85].

## Acknowledgments

This work was supported in part by the National Natural Science Foundation of China, the U.S. National Science Foundation, Air Force Office of Scientific Research, Army Research Office, Petroleum Research Fund, Research Corporation, and the Pittsburgh Supercomputing Center. We are indebted to many of our collaborators over the years including Y.S. Kivshar, D.N. Christodoulides, J. Xu, M. J. Ablowitz, M. Segev, P.G. Kevrekidis, D. Neshev, E.D. Eugenieva, and to many of our students and research fellows including X. Wang, A. Bezryadina, H. Martin, I. Makasyuk, D. Weinstein, C. Lou, J. Young, L. Tang, A. Fors, and A. Samodurov.

## References

1. D. N. Christodoulides, F. Lederer, and Y. Silberberg, "Discretizing light behaviour in linear and nonlinear waveguide lattices," *Nature* **424**, 817 (2003).
2. D. Campbell, S. Flach and Y.S. Kivshar, "Localizing energy through nonlinearity and discreteness," *Phys. Today* **57**, 43 (2004).
3. D. N. Christodoulides and R. I. Joseph, "Discrete self-focusing in nonlinear arrays of coupled waveguides," *Opt. Lett.* **13**, 794 (1988).
4. H. S. Eisenberg, Y. Silberberg, R. Morandotti, A. R. Boyd, and J. S. Aitchison, "Observation of discrete solitons in optical waveguide arrays," *Phys. Rev. Lett.* **81**, 3383 (1998).
5. R. Morandotti, H. S. Eisenberg, Y. Silberberg, M. Sorel, and J. S. Aitchison, "Self-Focusing and defocusing in waveguide arrays," *Phys. Rev. Lett.* **86**, 3296 (2001).
6. N. K. Efremidis, S. Sears, D. N. Christodoulides, J. W. Fleischer, and M. Segev, "Discrete solitons in photorefractive optically induced photonic lattices," *Phys. Rev. E* **66**, 046602 (2002).
7. J. W. Fleischer, T. Carmon, M. Segev, N. K. Efremidis, and D. N. Christodoulides, "Observation of discrete solitons in optically induced real time waveguide arrays," *Phys. Rev. Lett.* **90**, 023902 (2003).

8. J. W. Fleischer, M. Segev, N. K. Efremidis, and D. N. Christodoulides, "Observation of two-dimensional discrete solitons in optically induced nonlinear photonic lattices," *Nature* **422**, 147 (2003).
9. D. Neshev, E. Ostrovskaya, Y. Kivshar, and W. Krolikowski, "Spatial solitons in optically induced gratings," *Opt. Lett.* **28**, 710 (2003).
10. H. Martin, E. D. Eugenieva, Z. Chen, and D. N. Christodoulides, "Discrete solitons and soliton-induced dislocations in partially-coherent photonic lattices," *Phys. Rev. Lett.* **92**, 123902 (2004);
11. Z. Chen, H. Martin, E. D. Eugenieva, J. Xu, and A. Bezryadina, "Anisotropic enhancement of discrete diffraction and formation of two-dimensional discrete-soliton trains," *Phys. Rev. Lett.* **92**, 143902 (2004).
12. B. A. Malomed and P. G. Kevrekidis, "Discrete vortex solitons," *Phys. Rev. E* **64**, 026601 (2001).
13. J. Yang and Z. H. Musslimani, "Fundamental and vortex solitons in a two-dimensional optical lattice," *Opt. Lett.* **28**, 2094 (2003); Z. Musslimani and J. Yang, "Self-trapping of light in a two-dimensional periodic structure." *J. Opt. Soc. Am. B.* **21**, 973-981 (2004); J. Yang, "Stability of vortex solitons in a photorefractive optical lattice." *New Journal of Physics* **6**, 47 (2004).
14. D. N. Neshev, T. J. Alexander, E. A. Ostrovskaya, Y. S. Kivshar, H. Martin, I. Makasyuk, and Z. Chen, "Observation of discrete vortex solitons in optically-induced photonic lattices," *Phys. Rev. Lett.* **92**, 123903 (2004).
15. J. W. Fleischer, G. Bartal, O. Cohen, O. Manela, M. Segev, J. Hudock, D. N. Christodoulides, "Observation of vortex-ring discrete solitons in 2D photonic lattices," *Phys. Rev. Lett.* **92**, 123904 (2004).
16. J. D. Joannopoulos, R. D. Meade, and J. N. Winn, *Photonic Crystals: Molding the Flow of Light* (Princeton, NJ, 1995).
17. P. Russell, "Photonic crystal fibers," *Science* **299**, 358 (2003).
18. S. L. McCall, P. M. Platzman, R. Dalichaouch, D. Smith, and S. Schultz, "Microwave propagation in two-dimensional dielectric lattices," *Phys. Rev. Lett.* **67**, 2017 (1991); E. Yablonovitch, T. J. Gmitter, R. D. Meade, A. M. Rappe, K. D. Brommer, and J. D. Joannopoulos, "Donor and acceptor modes in photonic band structure," *Phys. Rev. Lett.* **67**, 3380 (1991); M. Bayindir, B. Temelkuran, and E. Ozbay, "Tight-Binding Description of the Coupled Defect Modes in Three-Dimensional Photonic Crystals," *Phys. Rev. Lett.* **84**, 2140 (2000).
19. F. Luan, A. K. George, T. D. Hedley, G. J. Pearce, D. M. Bird, J. C. Knight, and P. St. J. Russell, "All-solid photonic bandgap fiber," *Opt. Lett.* **29**, 2369 (2004).
20. A. Argyros, T. A. Birks, S. G. Leon-Saval, C. B. Cordeiro, F. Luan, and P. St. J. Russell, "Photonic bandgap with an index step of one percent," *Opt. Express* **13**, 309 (2005).
21. J. Schmidtke, W. Stille, and H. Finkelmann, "Defect mode emission of a dye doped cholesteric polymer network", *Phys. Rev. Lett.* **90**, 083902 (2003); J. S. Foresi, P. R. Villeneuve, J. Ferrera, E. R. Thoen, G. Steinmeyer, S. Fan, J. D. Joannopoulos, L. C. Kimerling, H. I. Smith, and E. P. Ippen, "Photonic-bandgap microcavities in optical waveguides," *Nature(London)* **390**, 143-145, (1997); S. Fan, P. R. Villeneuve, J. D. Joannopoulos, and H. A. Haus, "Channel Drop Tunneling through Localized States," *Phys. Rev. Lett.* **80**, 960 (1998).

22. X. Wu, A. Yamilov, X. Liu, S. Li, V. P. Dravid, R. P. H. Chang, and H. Cao, "Ultraviolet photonic crystal laser," *Appl. Phys. Lett.* **85**, 3657 (2004); O. Painter, R. K. Lee, A. Scherer, A. Yariv, J. D. O'Brien, P. D. Dapkus, and I. Kim, "Two-Dimensional Photonic Band-Gap Defect Mode Laser," *Science*, **284**, 1819(1999).
23. D. Mandelik, H. S. Eisenberg, Y. Silberberg, R. Morandotti, and J. S. Aitchison, "Band structure of waveguide arrays and excitation of Floquet-Bloch solitons," *Phys. Rev. Lett.* **90**, 53902 (2003).
24. N. K. Efremidis, J. Hudock, D. N. Christodoulides, J. W. Fleischer, O. Cohen, and M. Segev, "Two-Dimensional optical lattice solitons," *Phys. Rev. Lett.* **91**, 213906 (2003).
25. A. A. Sukhorukov, D. Neshev, W. Krolikowski, and Y. S. Kivshar, "Nonlinear Bloch-wave interaction and Bragg scattering in optically induced lattices," *Phys. Rev. Lett.* **92**, 093901 (2004).
26. U. Peschel, R. Morandotti, J. S. Aitchison, H. S. Eisenberg, and Y. Silberberg, "Nonlinearly induced escape from a defect state in waveguide arrays," *Appl. Phys. Lett.* **75**, 1348 (1999).
27. R. Morandotti, H. S. Eisenberg, D. Mandelik, Y. Silberberg, D. Modotto, M. Sorel, C. R. Stanley, and J. S. Aitchison, "Interactions of discrete solitons with structural defects," *Opt. Lett.* **28**, 834 (2003).
28. F. Fedele, J. Yang, and Z. Chen, "Defect modes in one-dimensional photonic lattices," *Opt. Lett.* **30**, 1506 (2005).
29. F. Fedele, J. Yang, and Z. Chen, "Properties of defect modes in one-dimensional optically-induced photonic lattices," *Stud. Appl. Math.*, **115**, 279 (2005).
30. X. Wang, Z. Chen and J. Yang, "Guiding light in optically-induced ring lattices with a low refractive index core," *Opt. Lett.* **31**, 1887 (2006).
31. I. Makasyuk, Z. Chen and J. Yang, "Band-gap guidance in optically induced photonic lattices with a negative defect," *Phys. Rev. Lett.*, **96**, 223903 (2006).
32. X. Wang, J. Young, Z. Chen, D. Weinstein, and J. Yang, "Observation of lower to higher bandgap transition of one-dimensional defect modes," *Opt. Express*, **14**, 7362-7367 (2006).
33. M. Soljacic, M. Segev, T. Coskun, D. N. Christodoulides, and A. Vishwanath, "Modulation instability of incoherent beams in noninstantaneous nonlinear media," *Phys. Rev. Lett.* **84**, 467 (2000).
34. T. H. Coskun, D. N. Christodoulides, Y.-R. Kim, Z. Chen, M. Soljacic, and M. Segev, "Bright Spatial Solitons on a Partially Incoherent Background", *Phys. Rev. Lett.* **84**, 2374 (2000); D. Kip, M. Soljacic, M. Segev, E. Eugenieva, D. N. Christodoulides, "Modulation Instability and Pattern Formation in Spatially Incoherent Light Beams", *Science* **290**, 495 (2000).
35. Z. Chen and K. MacCarthy, "Spatial soliton pixels from partially coherent light," *Optical Letters*, **27**, 2019 (2002); Z. Chen, K. MacCarthy, and H. Martin, "Photonic lattices induced by partially coherent light", *Optics and Photonic News*, December 2002.
36. M. Shih, Z. Chen, M. Mitchell, M. Segev, "Waveguides induced by one-dimensional photorefractive screening solitons," *J. Opt. Soc. Am. B*, **14**, 3091, 1997.

37. M. Mitchell, Z. Chen, M. Shih, and M. Segev, "Self-trapping of partially spatially incoherent light," *Phys. Rev. Lett.* **77**, 490 (1996).
38. Z. Chen, M. Mitchell, M. Segev, T.H. Coskun and D.N. Christodoulides, "Self-trapping of dark incoherent light beams", *Science*, **280**, 889, 1998; Z. Chen, M. Segev, and D. N. Christodoulides, "Experiments on partially coherent photorefractive solitons," in a special issue of *Journal of Optics A: Pure and Applied Optics*, **5**, S389, 2003.
39. J. Petter, J. Schrder, D. Trger, C. Denz, "Optical control of arrays of photorefractive screening solitons", *Opt. Lett.* **28**, 438 (2003); M. Petrovic, D. Trauer, A. Strinic, M. Belic, J. Schoder, C. Denz, "Solitonic lattices in photorefractive crystals", *Phys. Rev. E* **68**, 055601(R) (2003).
40. D.N. Neshev, Y. S. Kivshar, H. Martin, Z. Chen, "Soliton stripes in two-dimensional nonlinear photonic lattices", *Opt. Lett.* **29**, 486 (2004).
41. A.S. Desyatnikov, E.A. Ostrovskaya, Y.S. Kivshar, C. Denz, "Composite Band-Gap Solitons in Nonlinear Optically Induced Lattices", *Phys. Rev. Lett.* **91**, 153902 (2003).
42. A. Bezryadina, J. Young, Z. Chen, D. Neshev, A. Desyatnikov and Y. Kivshar, "Observation of angular momentum transfer and charge flipping due to nonlinear vortex-lattice interaction", *Optics Express*. **14**, 8317 (2006).
43. H. F. Talbot, *Philos. Mag.* **9**, 401 (1836).
44. R. Iwanow, D. A. May-Arrioja, D. N. Christodoulides, G. I. Stegeman, Y. Min, and W. Sohler *Phys. Rev. Lett.* **95**, 053902 (2005).
45. M. Segev, G. C. Valley, B. Crosignani, P. DiPorto, and A. Yariv, "Steady-State Spatial Screening Solitons in Photorefractive Materials with External Applied Field", *Phys. Rev. Lett.* **73**, 3211 (1994).
46. Z. Chen, M. Segev, T.H. Coskun and D.N. Christodoulides, "Observation of incoherently coupled photorefractive spatial soliton pair", *Opt. Lett.*, **21**, 1436 (1996).
47. J. Klinger, H. Martin, and Z. Chen, "Experiments on induced modulational instability of an incoherent optical beam," *Opt. Lett.* **26**, 271 (2001); Z. Chen, J. Klinger, and D. N. Christodoulides, "Induced modulation instability of partially spatially incoherent light with varying perturbation periods," *Phys. Rev. E* **66**, 66601 (2002).
48. Z. Chen, S. Sears, H. Martin, M. Segev, and D. N. Christodoulides, "Clustering of solitons in weakly correlated wavefronts," *Proc. Natl. Acad. Sci. U.S.A.* **99**, 5523 (2002).
49. D. Kip, M. Soljagic, M. Segev, S. M. Sears, and D. N. Christodoulides, "(1+1) - Dimensional modulation instability of spatially incoherent light," *J. Opt. Soc. Am. B* **19**, 502 (2002).
50. Z. Chen, H. Martin, A. Bezryadina, D. Neshev, Y. S. Kivshar, D. N. Christodoulides, "Experiments on Gaussian beams and vortices in optically induced photonic lattices," *J. Opt. Soc. Am. B* **22**, 1395 (2005).
51. Z. Chen, I. Makasyuk, A. Bezryadina, and J. Yang, "Observation of two-dimensional lattice vector solitons," *Opt. Lett.* **29**, 1656 (2004).
52. J. Yang, I. Makasyuk, A. Bezryadina, and Z. Chen, "Dipole solitons in optically-induced two-dimensional photonic lattices," *Opt. Lett.* **29**, 1662 (2004).

53. C. Lou, J. Xu, L. Tang, Z. Chen, and P. G. Kevrekidis, "Symmetric and antisymmetric soliton states in two-dimensional photonic lattices," *Opt. Lett.* **31**, 492 (2006).
54. J. Hudock, N. K. Efremidis, and D. N. Christodoulides, "Anisotropic diffraction and elliptic discrete solitons in two-dimensional waveguide arrays," *Opt. Lett.* **29**, 268 (2004).
55. D. N. Christodoulides, T. H. Coskun, M. Mitchell, and M. Segev, "Theory of Incoherent Self-Focusing in Biased Photorefractive Media," *Phys. Rev. Lett.* **78**, 646 (1997).
56. Z. Chen, H. Martin, E. D. Eugenieva, J. Xu, J. Yang, and D. N. Christodoulides, "Formation of discrete solitons in light-induced photonic lattices," focus issue in *Opt. Express*. **13**, 1816 (2005).
57. F. Lederer, S. Darmanyan, and A. Kobayakov, in *Spatial Optical Solitons*, S. Trillo and W. E. Torruellas, eds.(Springer-Verlag, New York, 2001).
58. M. J. Ablowitz and Z. H. Musslimani, "Discrete vector spatial solitons in a nonlinear waveguide array," *Phys. Rev. E* **65**, 056618 (2002).
59. J. Hudock, P. G. Kevrekidis, B. A. Malomed, and D. N. Christodoulides, "Discrete vector solitons in two-dimensional nonlinear waveguide arrays: Solutions, stability, and dynamics," *Phys. Rev. E* **67**, 056618 (2003).
60. J. Meier, J. Hudock, D. N. Christodoulides, G. Stegeman, Y. Silberberg, R. Morandotti, and J. S. Aitchison, "Discrete vector solitons in Kerr nonlinear waveguide arrays," *Phys. Rev. Lett.* **91**, 143907 (2003).
61. J. Yang, I. Makasyuk, A. Bezryadina, and Z. Chen, "Dipole and quadrupole solitons in optically-induced two-dimensional photonic lattices: theory and experiment," *Stud. Appl. Math.* **113**, 389 (2004).
62. P. G. Kevrekidis, A. R. Bishop, and K. Rasmussen, "Twisted localized modes," *Phys. Rev. E* **63**, 036603 (2001).
63. A. A. Sukhorukov and Y.S. Kivshar, "Spatial optical solitons in nonlinear photonic crystals," *Phys. Rev. E* **65**, 036609 (2002).
64. P. G. Kevrekidis, B. A. Malomed, A. R. Bishop, "Bound states of two-dimensional solitons in the discrete nonlinear Schrodinger equation," *J. Phys. A* **34**, 9615 (2001).
65. S.R. Singh and D.N. Christodoulides, "Evolution of spatial optical solitons in biased photorefractive media under steady state conditions," *Opt. Comm.* **118**, 569 (1995).
66. P. G. Kevrekidis, Z. Chen, B. A. Malomed, D. J. Frantzeskaki, M. I. Weinstein, "Spontaneous symmetry breaking in photonic lattices: Theory and experiment," *Phys. Lett. A* **340**, 275 (2005).
67. S. Darmanyan, A. Kobayakov, and F. Lederer, "Stability of strongly localized excitations in discrete media with cubic nonlinearity," *JETP* **86**, 682 (1998).
68. G. A. Swartzlander and C.T. Law, "Optical vortex solitons observed in Kerr nonlinear media", *Phys. Rev. Lett.* **69**, 2503 (1992).
69. Z. Chen, M. Segev, D.W. Wilson, R.E. Muller and P.D. Maker "Self-trapping of an optical vortex by use of bulk photovoltaic effect", *Physical Review Letters*, **78**, 2948 (1997); Z. Chen, M. Shih, M. Segev, D.W. Wilson, R.E. Muller and P.D. Maker, "Steady-state vortex screening-solitons formed in photorefractive media", *Opt. Lett.*, **22**, 1751 (1997).

- 
70. A. S. Desyatnikov, Y. S. Kivshar, L. Torner, in *Prog. in Optics*, **47**, E.Wolf ed. (North-Holland 2005).
  71. A. Bezryadina, E. Eugenieva, and Z. Chen, "Self-trapping and flipping of double-charged vortices in optically induced photonic lattices," *Opt. Lett.* **31**, 2458 (2006).
  72. B. Baizakov, B. A. Malomed, and M. Salerno, "Multidimensional solitons in periodic potentials", *Europhys. Lett.* **63**, 642 (2003).
  73. P.G. Kevrekidis, B.A. Malomed, Z. Chen and D.J. Frantzeskakis, "Stable higher charge vortices in the discrete nonlinear Schrodinger equation", *Phys. Rev. E.* **70**, 056612 (2004).
  74. T. J. Alexander, A. A. Sukhorukov, and Yu. S. Kivshar, "Asymmetric vortex solitons in nonlinear periodic lattices", *Phys. Rev. Lett.* **93**, 063901 (2004).
  75. A. Ferrando, M.Zacares. M. Garcia-March, J. A. Monsoriu, and P. F. de Cordoba, "Vortex Transmutation", *Phys. Rev. Lett.* **95**, 123901 (2005).
  76. A. Smerzi, A. Trombettoni, P. G. Kevrekidis, and A. R. Bishop, "Dynamical Superfluid-Insulator Transition in a Chain of Weakly Coupled Bose-Einstein Condensates," *Phys. Rev. Lett.* **89**, 170402(2002).
  77. P. G. Kevrekidis, G. Theocharis, D. J. Frantzeskakis, and B. A. Malomed, "Feshbach resonance management for Bose-Einstein condensates," *Phys. Rev. Lett.* **90**, 230401(2003).
  78. J. Yang. I. Makasyuk, H. Martin, P. G. Kevrekidis, B. A. Malomed, D. J. Frantzeskakis, and Z. Chen, "Necklace-like solitons in optically induced photonic lattices," *Phys. Rev. Lett.* **94**, 113902 (2005).
  79. R. Iwanow, R. Schiek, G. I. Stegeman, T. Pertsch, F. Lederer, Y. Min, and W. Sohler, "Observation of discrete quadratic solitons," *Phys. Rev. Lett.* **93**, 113902 (2004).
  80. A. Fratolocci, G. Assanto, K. A. Brzdakiewicz, and M. A. Karpierz, "Discrete propagation and spatial solitons in nematic liquid crystals," *Opt. Lett.* **29**, 1530 (2004).
  81. Y. V. Kartashov, V. A. Vysloukh, and L. Torner, "Rotary solitons in Bessel optical lattices," *Phys. Rev. Lett.* **93**, 093904 (2004).
  82. Z. Xu, Y. V. Kartashov, L. Torner, V. A. Vysloukh, "Reconfigurable directional couplers and junctions optically induced by nondiffracting Bessel beams," *Opt. Lett.* **30**, 1180 (2005).
  83. X. Wang, Z. Chen and P.G. Kevrekidis, "Discrete solitons and soliton rotation in periodic ring lattices", *Phys. Rev. Lett.* **96**, 083904 (2006).
  84. N. M. Litchinitser, A. K. Abeeluck, C. Headley, and B. J. Eggleton, "Antiresonant reflecting photonic crystal optical waveguides," *Opt. Lett.* **27**, 1592 (2002).
  85. Y. S. Kivshar and G. P. Agrawal, *Optical Solitons* (Academic Press, New York, 2003); S. Aitchison, D. Christodoulides, and L. Torner, "Spatial Optical Solitons", Focus issue, *J. Opt. Soc. Am. B* **22**, 1346 (2005); D. Christodoulides, "Discrete solitons in nonlinear optics", Focus issue, *Opt. Express* **13**, 1761 (2005); Y. Kartashov, L. Torner and D. Christodoulides and V. Vysloukh, "Soliton control in optical lattices", *Progress in Optics*, to appear.